Spatiotemporal characteristics of calcium dynamics in astrocytes

Minchul Kang[1] and Hans G. Othmer[2,a)]
[1]*Department of Molecular Physiology and Biophysics, Vanderbilt University School of Medicine, Nashville, Tennessee 37232, USA*
[2]*School of Mathematics, University of Minnesota, Minneapolis, Minnesota 55455, USA*

(Received 21 February 2009; accepted 24 July 2009; published online 18 September 2009)

Although Ca_i^{2+} waves in networks of astrocytes *in vivo* are well documented, propagation *in vivo* is much more complex than in culture, and there is no consensus concerning the dominant roles of intercellular and extracellular messengers [inositol 1,4,5–trisphosphate (IP_3) and adenosine-5′-triphosphate (ATP)] that mediate Ca_i^{2+} waves. Moreover, to date only simplified models that take very little account of the geometrical struture of the networks have been studied. Our aim in this paper is to develop a mathematical model based on realistic cellular morphology and network connectivity, and a computational framework for simulating the model, in order to address these issues. In the model, Ca_i^{2+} wave propagation through a network of astrocytes is driven by IP_3 diffusion between cells and ATP transport in the extracellular space. Numerical simulations of the model show that different kinetic and geometric assumptions give rise to differences in Ca_i^{2+} wave propagation patterns, as characterized by the velocity, propagation distance, time delay in propagation from one cell to another, and the evolution of Ca^{2+} response patterns. The temporal Ca_i^{2+} response patterns in cells are different from one cell to another, and the Ca_i^{2+} response patterns evolve from one type to another as a Ca_i^{2+} wave propagates. In addition, the spatial patterns of Ca_i^{2+} wave propagation depend on whether IP_3, ATP, or both are mediating messengers. Finally, two different geometries that reflect the *in vivo* and *in vitro* configuration of astrocytic networks also yield distinct intracellular and extracellular kinetic patterns. The simulation results as well as the linear stability analysis of the model lead to the conclusion that Ca_i^{2+} waves in astrocyte networks are probably mediated by both intercellular IP_3 transport and nonregenerative (only the glutamate-stimulated cell releases ATP) or partially regenerative extracellular ATP signaling. © *2009 American Institute of Physics*. [DOI: 10.1063/1.3206698]

Calcium (Ca^{2+}) is one of the most versatile and widely used second-messenger molecules and plays a pivotal role in neurotransmission, muscle contraction, gene expression, and a variety of other intracellular processes.[13,37] Because high levels of intracellular calcium are toxic, and because it cannot be degraded as many other signaling molecules are, cells control the intracellular calcium level at around 100 n*M* (compared to millimolar extracellular levels) by buffering, sequestration in specialized compartments, and by expulsion to the extracellular space.[37,110,115] In addition to intracellular homeostatic mechanisms to control Ca_i^{2+}, sophisticated intracellular signal transduction pathways that involve different proteins modulated by Ca^{2+} have evolved for communication between cells.[7,38,39,41,42,60–62,70,100,119] In the central nervous system, glial cells (collectively, astrocytes, oligodendrocytes, and microglia), which are 10–15 times more numerous than neurons, make up about half of the total brain weight. Astrocytes, which are the dominant glial cell type, had been regarded as maintenance and support cells for neurons until recently, because they lack sodium channels and are electrically nonexcitable.[117] It has been found experimentally that Ca_i^{2+} waves propagate through networks of astrocytes, and there is a great deal of interest in understanding their role in the brain. In this paper we develop mathematical models that shed light on what factors control the spread of such waves.

I. INTRODUCTION

A. Glutamate induced Ca_i^{2+} mobilization in astrocytes

A major metabotropic pathway from agonist to calcium changes is via receptor-activated G proteins that initiate production of inositol 1,4,5–trisphosphate (IP_3), which then binds to IP_3 receptors on calcium channels in the membrane of the endoplasmic reticulum (ER), an intracellular Ca^{2+} store. Calcium release from the ER is terminated by Ca^{2+} inhibition of channel opening at high concentrations[14] and pumps restore Ca_i^{2+} to resting levels. Typically the reuptake makes the Ca^{2+} signal a transient "spike" and allows the cell to maintain very low levels of resting Ca_i^{2+}.

It was shown previously that the intracellular network that controls Ca_i^{2+} dynamics is comprised of four modules [cf. Fig. 1(a)] that can be summarized as follows:[67] (1) the ligand and receptor kinetics at the plasma membrane (the input module), (2) a G_q-type G-protein-activated module in which activated phospholipase C (PLC) leads to the production of IP_3 and diacylglycerol (DAG) from phosphatidylinositol-biphosphate (PIP_2) (the amplifying

a)Author to whom correspondence should be addressed. Electronic mail: othmer@math.umn.edu. Telephone: +1 (612) 624-8325.

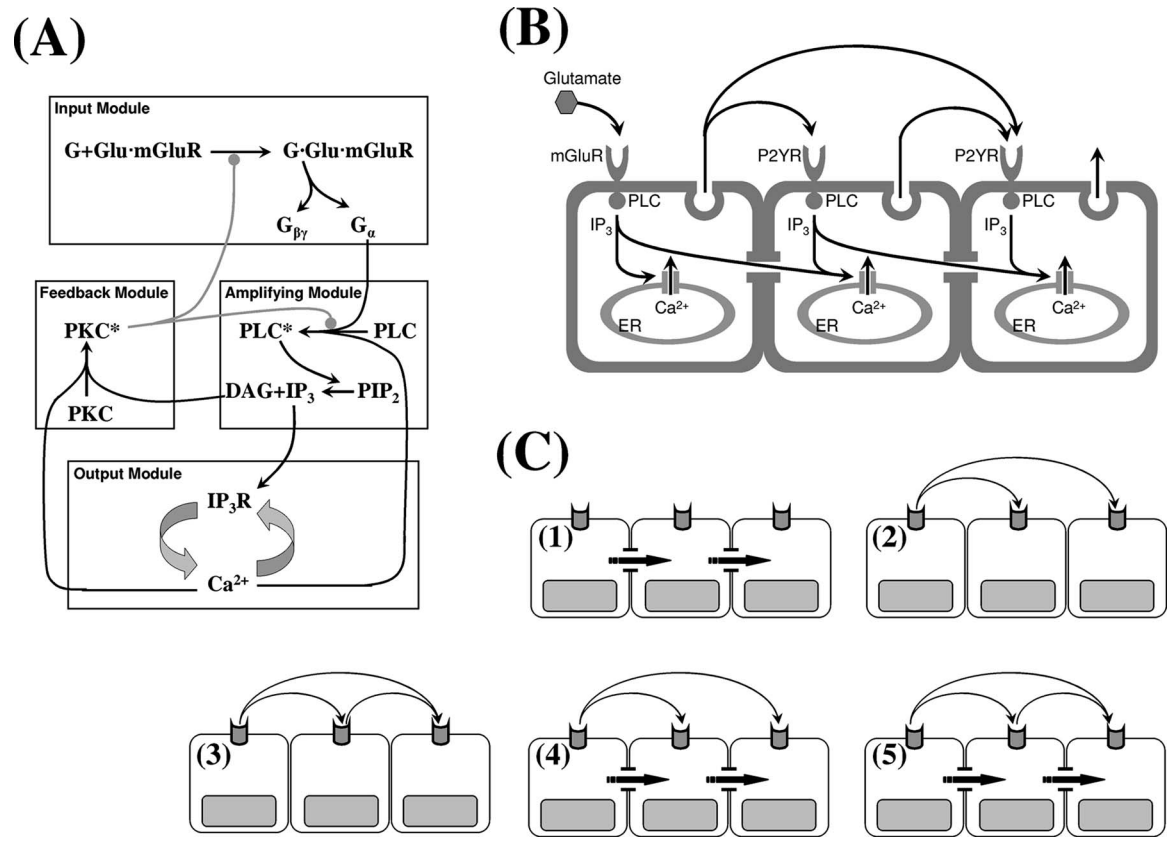

FIG. 1. (a) The modular representation of the glutamate-induced Ca^{2+} release pathway. (b) A schematic overview of the possible mechanism of Ca_i^{2+} wave propagation in an astrocyte network. (c) Case studies of Ca_i^{2+} wave propagation under all the possible combination of intracellular and extracellular messengers: (1) direct coupling and no extracellular signal, (2) nonregenerative extracellular signal and no direct coupling, (3) regenerative extracellular signal and no direct coupling, (4) direct coupling and nonregenerative extracellular signal, and (5) regenerative extracellular signal and direct coupling. Note that autocrine ATP signaling is neglected for the glutamate-stimulated cell.

module), (3) an IP_3/IP_3-receptor system that controls the Ca^{2+} release from the ER by calcium-induced calcium release (CICR) (the output module), and (4) a feedback module involving DAG-Ca^{2+} activation of protein kincase C (PKC), which leads to downregulation of receptors and PLC (the feedback module). The input module receives stimulatory ligand and inhibitory PKC signals as inputs and produces G_α and $G_{\beta\gamma}$ as outputs, the former of which serves as an input to the amplifying module. The amplifying module produces its outputs, IP_3 and DAG, from the hydrolysis of PIP_2 by G_α-activated PLC. While soluble IP_3 diffuses into the cytoplasm and functions as an input to the output module, hydrophobic DAG stays at the inner leaflet of the plasma membrane. The output module comprises the Ca^{2+} handling mechanisms such as IP_3-stimulated release from the ER and Sarco/Endoplasmic Reticulum calcium ATPase (SERCA) uptake and outputs Ca_i^{2+}. Finally, the feedback module receives Ca_i^{2+} and DAG as inputs and produces the activated state of PKC, which downregulates the activity of input and amplifying modules. A detailed model for calcium dynamics in isolated cells based on this modular decomposition was derived and analyzed earlier.[67]

B. Ca^{2+} wave propagation in astrocyte networks

It is now believed, after numerous reports of Ca_i^{2+} waves in astrocyte networks following various stimuli,[89,93,97,84,86,24,45,95] that astrocytes modulate neural network activities via astro-astro and astroneuronal cross-talk, although their physiological roles *in vivo* are still subject to debate.[1,37,45,43,35,83,116,78,99] One example of the cross-talk is reflected in adenosine-5′-triphosphate (ATP)-mediated calcium waves, which demonstrate the coupling between intracellular calcium dynamics and cell-cell communication via the extracellular space.[1,37,56] Such waves, which typically decay in time and in space as they propagate, have a maximal propagation range of 200–350 μm and a maximal velocity of 15–27 $\mu m^2/s$.[15,113,120,82,18]

There is substantial evidence that Ca_i^{2+} waves in astrocytes are mediated by direct coupling between astrocytes via transport through gap junctions[49,105,114,94] and/or by paracrine ATP signaling via the extracellular space.[26,54,18,17,65,103] The mode of communication used depends on the astrocyte subtype,[45] and there is a significant diversity with respect to interactions with surrounding cells.[1] For example, gap junctional coupling appears to be important in astrocytes in the neocortex, while paracrine ATP signaling can induce Ca_i^{2+} waves independent of gap junctional coupling in astrocytes in the hippocampus.[45] However, the findings that Ca^{2+} waves can propagate between physically separated astrocytes[54,58,11] and in cultured astrocytes in which gap junctional coupling was pharmacologically impaired[53,63] suggest that extracellular ATP signaling plays a major role in *in vitro*, although it

may not be the only mode. The overview of these possible mechanisms of Ca_i^{2+} wave propagation in an astrocyte network is described in Fig. 1(b).

Just as Ca_i^{2+} is strictly regulated by cells, the level of ATP is also tightly controlled, but the relative levels are reversed. While cytosolic ATP is >5 mM in most cells,[50,51] extracellular [ATP] is kept around 1 nM (Ref. 64) by various enzymes. Thus large amounts of ATP can be released into the extracellular space under pathological conditions such as tissue injury, cell lysis, and cell ischemia.[3,108] Under physiological conditions, cytosolic ATP can be released via transmembrane transport in response to receptor activation in both vascular smooth muscle cells and endothelial cells.[96,98,68,123] In most neurons, ATP is stored in vesicles with neurotransmitters and coreleased.[16,40] Under experimental conditions various environmental stressors, such as a mechanical stress, have been used as stimuli to release ATP. It has also been reported that ATP may be released via spontaneous changes in cell volume via volume-regulated anion channels (VRACs).[92] Similarly, there are multiple possible ATP release mechanisms in astrocytes. Hemichannel-mediated ATP release,[25,4,103,20,65,2] vesicular release,[22,18,17,122] and P2X7 ATP receptor mediated release[104] have been postulated, but recent evidence suggests that vesicular release is the most probable mechanism.[18,17] At present there is no evidence of transporter-mediated cellular uptake of ATP, even though nucleotides and nucleobases are taken up by several transport systems.[52]

Extracellular ATP can reach biologically active levels from nanomolar to micromolar concentrations near a release site[50,73,82,121] and participates in various signaling processes,[34,32,69] but the half-life of extracellular ATP is very short due to the presence of potent degrading enzymes. It was reported that ATP reaches a local peak as high as 10–75 μM (Refs. 109, 121, and 82) and that the ATP "front" diffuses outward at about 41 μm/s, which exceeds the speed of 28 μm/s for the Ca_i^{2+} wave front.[82] The maximal detectable ATP spread ranges from 84 to 120 μm depending on the stimulus source.[82,4,58] The measured diffusion coefficient for the extracellular ATP ranges from 160 to 330 $\mu m^2/s$,[91,59,81] which is much slower than in the cytosol. Estimated degradation rates for ATP in the extracellular space of astrocytes range from 3.466/s to 4×10^{-4}/s.[64]

Extracellular ATP can bind to metabotropic ATP receptors (P2YRs) on cells, and at sufficiently high levels it can initiate signaling cascades, including Ca_i^{2+} release. The effective dosage of ATP for astrocyte Ca_i^{2+} response has been reported to be 0.74–3 μM.[82,64] There are two distinct ATP binding sites on P2YR—low affinity site and high affinity site—the former having a $K_d=20\pm5$ μM with a total concentration of $B_{max}=150$ n$M/10^6$ cells of P2YR, while the latter having a $K_d=2.5\pm0.2$ μM with $B_{max}=52$ n$M/10^6$ cells and a dissociation rate of 1.2×10^{-3}/s.[76] [Concentrations are based on the volumes of rat and human astrocytes, which have been estimated as 66×10^3 and 18×10^5 μm^3 (Refs. 85 and 21).] In the model we fix the ATP release rate constant so that the peak ATP concentration is ~30 μM. Since there are considerable differences in ATP degradation rates reported in the literature, the extracellular ATP decay rate is treated as a parameter to control the extracellular ATP level. For simplicity, we will not distinguish the two different ATP binding sites on P2YR and set $B_{max}=0.1$ μM and $K_d=10$ μM.

C. The rationale for the model structure

Ca_i^{2+} increases are often found to be spatially synchronized in cultured astrocytes, which usually form an adherent cell monolayer that is well approximated as a rectangular tessellation of a two-dimensional (2D) domain.[37,45,11] This has led to suggestions that long-range propagation of Ca_i^{2+} in cultured astrocytes is doubtful under physiological conditions.[45,1] However, *in vivo* astrocytes are interconnected by well-developed fine processes that constrain the waves to propagate along certain routes and provide weaker gap-junctional connectivity between cells. Even for the same cell type, differences exist between cultured astrocytes and astrocytes *in vivo*, and as a result, there are conflicting opinions concerning the roles played by intercellular and extracellular messengers in astrocytic Ca_i^{2+} waves. As we show later, using a realistic morphology has important implications for complex network dynamics, although other factors also have significant effects. Our results suggest that morphological differences in cultured and intact astrocytes can cause different Ca_i^{2+}, IP_3, and ATP wave propagation patterns in terms of propagation velocity, propagation distance, amplitude, and delays between cells.

Many theoretical studies have been done to understand the phenotypical properties of Ca_i^{2+} waves reported for different cell types in various contexts.[60,10] For example, it is known how to predict the range of propagation in a highly simplified model of gap-junction-coupled cells.[5] However, to our knowledge no studies have considered realistic morphological differences between cells in different experimental studies. We considered a realistic yet simple mathematical model of Ca_i^{2+} elevation and wave propagation in two different geometries mimicking astrocytic networks *in vivo* and *in vitro* and tested it under various scenarios of Ca_i^{2+} wave propagation [Fig. 1(c)] based on a number of simplifying assumptions. First, we assumed that sustained glutamate stimulus is locally restricted in one cell, yet the glutamate concentration is high enough so that ATP released from neighboring astrocytes does not influence the Ca_i^{2+} response kinetics in the glutamate-stimulated cell. Second, all the astrocytes share identical physiological properties, which means that the same system of partial differential equations (PDEs) is valid for all the cells. Third, the distribution of ER is homogeneous throughout the cell body and processes of an astrocyte, i.e., the shape of the ER network matches the shape of an astrocyte. Fourth, P2YRs are also uniformly distributed over the cell body and processes of an astrocyte, and gap junctions may exist between adjacent astrocytes. Finally, we assume that the only difference between astrocytes *in vivo* and *in vitro* is in their morphology.

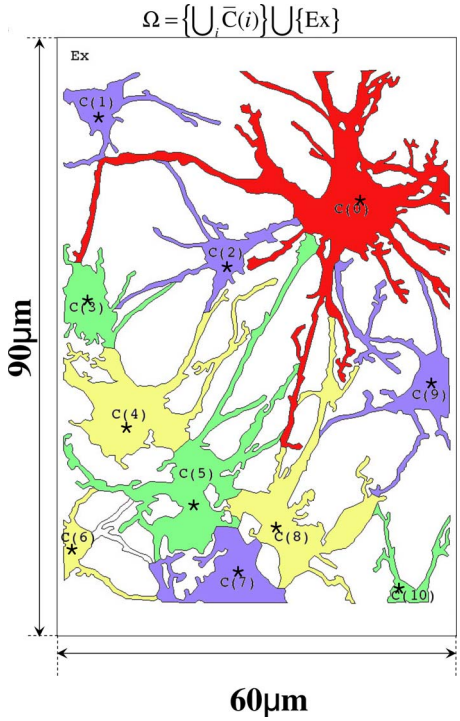

FIG. 2. (Color online) The astrocytic network geometry used in the *in vivo* model. Here and in the simplified model, C(0) is the cell stimulated by glutamate. The extracellular space is defined as $\Omega = \{\cup_i \bar{C}(i)\} \cup \{Ex\}$, where $\bar{C}(i)$ is the extracellular domain above C(i) and Ex is the cell free space.

II. THE MATHEMATICAL MODEL FOR Ca_i^{2+} WAVES

A. An overview of the spatial model

In the previous study,[67] a model of ligand-induced intracellular Ca^{2+} oscillations was developed and analyzed to understand the bifurcation structure of the different types of Ca_i^{2+} oscillations, particularly sinusoidal Ca_i^{2+} oscillations and baseline spiking, in terms of the role of PKC and PLC in determining the intracellular level of IP_3. Our objective here is to extend this to allow different modes of cell-cell communication, either directly via gap junctions or indirectly via the extracellular space. The goal is to develop a PDE model in order to understand Ca_i^{2+} wave propagation through an astrocytic network and ATP wave propagation in the extracellular space. As previously mentioned, substantial differences in Ca_i^{2+} waves were reported among different subtypes of astrocytes that result from the diversity of interactions with surrounding cells.[45] The differences are even larger between astrocytes *in vitro* (cultured) and *in vivo*.[45]

To determine how the different configurations of astrocyte network geometries influence Ca_i^{2+} wave propagation, the PDE model must be solved numerically in both realistic (*in vivo*) and simplified (*in vitro*) geometries for astrocyte networks, assuming only morphological differences between cultures and intact astrocytes (Fig. 2). In both cases, simulations under all possible combinations of direct coupling using an intracellular messenger (IP_3) and indirect communication using an extracellular messenger (ATP) were done to study the properties of Ca_i^{2+} waves. The cases considered are (1) direct coupling and no extracellular signal, (2) nonregenerative extracellular signal and no direct coupling, (3) regenerative extracellular signal and no direct coupling, (4) direct coupling and nonregenerative extracellular signal, and (5) regenerative extracellular signal and direct coupling [Fig. 1(c)].

B. Simplification of the intracellular temporal model

It can be shown that the full temporal model studied earlier[67] can be reduced to interactions between the key component in each of the modules, namely, IP_3, IP_3R, Ca^{2+}, and PKC. Formally, this can be done by introducing a time scale $\bar{t} = k_{-RCC}t$, converting the ordinary differential equation (ODE) system into nondenominational form to identify fast and slow steps as measured by the sizes of nondimensional groups and applying the pseudosteady state hypothesis to reduce some ODEs to algebraic equations.[47,66] By simplifying the resulting algebraic-differential equations we obtain a system that captures the slow dynamics to leading order in the small parameter. This leads to the following four-dimensional system:

$$\begin{aligned}
\frac{dP}{dt} &= \frac{k_1 C}{(1+k_2 K)} - k_3 P, \\
\frac{dK}{dt} &= k_4 C(K_T - K) - k_5 K, \\
\frac{dR}{dt} &= \frac{k_6 P C^2 (R_T - R)}{1 + k_7 P(1 + k_8 C)} - k_9 R, \\
\frac{dC}{dt} &= k_{10}\left(1 + \frac{k_{11} P C (R_T - R)}{1 + k_7 P(1 + k_8 C)}\right)(k_c - C) - \frac{k_{12} C^2}{C^2 + k_{p2}^2},
\end{aligned} \tag{1}$$

where P, K, R, and C represent the concentrations of IP_3, $Ca^{2+}\cdot PKC$ complex, $Ca^{2+}\cdot Ca^{2+}\cdot IP_3\cdot IP_3R$, and Ca_i^{2+}. The parameters that appear in Eq. (1) are given in Table I. Notice that C couples the first two equations to the last two, whereas P couples the last two to the first two. The reader can interpret the equations in terms of the interactions between the modules. For example, K, which arises from the feedback, affects the output via the first term in the first equation. The inhibitory feedback pathway of PKC Ca_i^{2+} dynamics is well documented in various studies.[8,30,31,29,112,6,28,46,23,80] Further discussion of the physical interpretation of Eq. (1) can be found in Appendix A and Ref. 66.

C. Geometry of the astrocyte networks

We later derive equations for waves in cultured astrocytes and for *in vivo* networks and here describe the geometry we use. Cultured astrocytes are often confluent, and to understand waves in this context we consider a finite line of cells wherein each is coupled to its nearest neighbors via gap junctions, as shown in Fig. 1(b). This line of cells is covered by a thin extracellular space that extends above and to the end of the line, in which ATP can diffuse, and we homogenize this system in the vertical direction so as to reduce it to 2D system of coupled squares of 15×15 μm^2 with fluid layer above it. We solve the equations both within the squares and in the exterior fluid layer using equations and

TABLE I. Parameters and their meaning. In the simplified geometry (*in vitro* model), $k_{\text{perm }P}=1$ were used (*). For IP_3 mediated Ca_i^{2+} wave (without ATP binding kinetics), $k_{\text{in}}=0$ was chosen (†), while $k_{\text{perm }P}=0$ was used to study ATP mediated Ca_i^{2+} wave without IP_3 diffusion (‡).

Parameter	Unit	Meaning	Value
D_A	$\mu m^2\ sec^{-1}$	Diffusion coefficient of ATP in extracellular space	330
D_P	$\mu m^2\ sec^{-1}$	Diffusion coefficient of IP_3	300
D_K	$\mu m^2\ sec^{-1}$	Diffusion coefficient of $Ca^{2+}\cdot PKC$	30
D_C	$\mu m^2\ sec^{-1}$	Effective diffusion coefficient of Ca_i^{2+}	30
k_1	sec^{-1}	Ca^{2+} dependence of IP_3 production	4.7994
k_2	μM^{-1}	PKC dependence of IP_3 production	0.0943
k_3	sec^{-1}	IP_3 degradation rate	2.5000
k_4	$\mu M^{-1}\ sec^{-1}$	Rate constant for PKC and Ca^{2+} binding	0.6000
k_5	sec^{-1}	$K\ (\overline{Ca^{2+}\cdot PKC})$ degradation rate	0.5000
k_6	$\mu M^{-2}\ sec^{-1}$	Binding rate constant for IP_3, $2Ca^{2+}$	139.09
k_7	μM^{-1}	Affinity constants for IP_3, $\overline{IP_3R}$	8.5000
k_8	μM^{-1}	Affinity constants for Ca^{2+}, $\overline{IP_3\cdot IP_3R}$	9.0909
k_9	sec^{-1}	$R(\overline{IP_3\cdot IP_3R\cdot Ca^{2+}\cdot Ca^{2+}})$ degradation rate	0.2100
k_{10}	sec^{-1}	Basal Ca^{2+} release rate from ER	0.0185
$\tilde{k}_{11}$	μM^{-2}	Affinity constant for C, P, and free IP_3R	·
$\bar{k}_{11}$	$\mu M^{-1}\ sec^{-1}$	Ca^{2+} release rate from IP_3R Ca^{2+} channels	·
k_{11}	μM^{-3}	$\bar{k}_{11}\tilde{k}_{11}/k_{10}$	15841
k_{12}	$\mu M\ sec^{-1}$	The maximal Ca^{2+} pumping rate	7.5000
k_c	μM	Volume averaged Ca^{2+} concentration	7.0000
k_{p2}	μM	Ca^{2+} sensitivity of the SERCA pump	0.1300
K_T	μM	Total K concentration	1.0000
R_T	μM	Total R concentration	0.8000
A_T	μM	ATP concentration in the cytosol	5000
k_{in}	sec^{-1}	Rate of ATP induced IP_3 production	$30/0^{\dagger}$
$k_{-\text{ATP}}$	sec^{-1}	ATP decay rate in extracellular space	1
$B_{\max}$	μM	The total concentration of P2YR	0.1
K_d	μM	Dissociation constant of ATP and P2YR	10
k_{ATP}	sec^{-1}	Maximal ATP release rate	0.184
γ	μm^{-1}	Extracellular volume dependent parameter	1.087
ρ	μM	IP_3 dependency parameter in ATP release	10
$k_{\text{perm }P}$	$\mu m/s$	Gap junctional permeability for IP_3	$2/1^{*}/0^{\ddagger}$
L	μm	The height of extracellular space	0.9

boundary conditions given later. Similar simplified model geometry was also studied extensively in Refs. 11, 101, 102, and 12.

The geometry of a realistic *in vivo* astrocyte network is very complicated, as shown in Fig. 2, and some simplifications are necessary. From the morphological point of view, astrocytes *in vivo* have well developed processes in both number and size covering most of the dendrites, axons, and synapses, as well as the larger soma.[1,21,85] To capture these characteristics, a realistic astrocyte network in $60\times 90\ \mu m^2$ rectangular domain was considered which was modified from original confocal immunofluorescence images of the vitreal surface of the rat retina.[81] The locations at which C_i, P_i, and A in C(i) were measured were marked as ⋆ [Fig. 2(b)], where A represents extracellular ATP concentration. The distance between measuring point from C(0) in descending order are C(2), C(9), C(1), C(3), C(4), C(8), C(5), C(10), C(7), and C(6) with distances 20.3, 29.8, 40.4, 42.4, 46.4, 49.3, 50.3, 58.2, 59.3, and 64.76 (μm). This system is also treated as having been homogenized the vertical direction, and equations given later are solved in the domain defined by the cells and that defined by the extracellular space. Here there is an additional difficulty, in that to be entirely faithful to the *in vivo* geometry we should treat the system as a two phase system (cell and fluid) as above, but here the fraction of the phases varies from point to point. This extension significantly complicates the problem computationally, and this will be pursued elsewhere.

Several lines of evidence indicate that gap junctional hemichannels play an important role by providing a direct path to second messengers such as IP_3.[15,49,72,105,114] A portion of mobilized Ca_i^{2+} also diffuses through the gap junctional hemichannels. However, due to various of Ca^{2+} buffer proteins in the cytosol, the amount is negligible and we ignore diffusion of Ca_i^{2+} between cells.[110,9] We assume that astrocytic gap junctions are located at the end of astrocytic processes as well as on the part of the boundary where astrocyte bodies.[79] Because it was hard to distinguish different cells from the image, the cell boundaries other than processes in the model were simply assigned. It was also assumed that the ATP receptors are present over the entire cell surface, although some studies indicate that a localization of ATP receptors either in an astrocyte cell body or processes could be specific to the astrocyte subtype.[48,90]

D. The governing equations for the spatial model

Let C(0) be a cell stimulated by glutamate (parametrized by k_1) and C(i), $i \neq 0$ be the surrounding cells (Fig. 2), and let X_i denote a quantity X in the i^{th} cell. In the subdomain C(0) (Fig. 2), for $t>0$,

$$\frac{\partial P_0}{\partial t} = D_P \Delta P_0 + \frac{k_1 C_0}{1+k_2 K_0} - k_3 P_0$$

$$\frac{\partial K_0}{\partial t} = D_K \Delta K_0 + k_4 C_0 (K_T - K_0) - k_5 K_0,$$

$$\frac{\partial R_0}{\partial t} = \frac{k_6 P_0 C_0^2 (R_T - R_0)}{1+k_7 P_0 (1+k_8 C_0)} - k_9 R_0, \tag{2}$$

$$\frac{\partial C_0}{\partial t} = D_C \Delta C_0 + k_{10}\left(1 + \frac{k_{11} C_0 P_0 (R_T - R_0)}{1+k_7 P_0 (1+k_8 C_0)}\right)(k_c - C_0) - \frac{k_{12} C_0^2}{C_0^2 + k_{p2}^2},$$

where R_0 is assumed to be immobile ($D_R=0$). The initial conditions on C(0)$\times\{t=0\}$ are given by

$$P_0(x,0)=0 \quad K_0(x,0)=0$$
$$R_0(x,0)=0 \quad C_0(x,0)=0.02. \tag{3}$$

Wherever cell C(0) meets other cells we impose the boundary conditions

$$-D_P \frac{\partial P_0}{\partial n} = k_{\text{perm } P}(P_0 - P_i),$$
$$\frac{\partial X}{\partial n} = 0 \quad \text{for } X = K_0, R_0, C_0, \tag{4}$$

while all other boundaries are impermeable to all species. When we consider extracellular messenger-mediated Ca_i^{2+} waves without IP_3 diffusion between cells, we simply set $k_{\text{perm } P}=0$.

Since ATP affects Ca^{2+} wave propagation via binding to P2YR, the equation for IP_3 involves an input that depends on ATP binding kinetics ($B_{\max}=0.1\ \mu M$, $K_d=10\ \mu M$) as well as on Ca_i^{2+} (C_i) and PKC (K_i). A similar term is absent from the glutamate-stimulated cell because we neglect the ATP stimulation relative to that by glutamate. Therefore,

$$\frac{\partial P_i}{\partial t} = D_P \Delta P_i + k_{\text{in}} \frac{B_{\max} A}{K_d + A} \frac{C_i}{1+k_2 K_i} - k_3 P_i,$$

$$\frac{\partial K_i}{\partial t} = D_K \Delta K_i + k_4 C_i (K_T - K_i) - k_5 K_i,$$

$$\frac{\partial R_i}{\partial t} = \frac{k_6 P_i C_i^2 (R_T - R_i)}{1+k_7 P_i (1+k_8 C_i)} - k_9 R_i, \tag{5}$$

$$\frac{\partial C_i}{\partial t} = D_C \Delta C_i + k_{10}\left(1 + \frac{k_{11} C_i P_i (R_T - R_i)}{1+k_7 P_i (1+k_8 C_i)}\right)(k_c - C_i) - \frac{k_{12} C_i^2}{C_i^2 + k_{p2}^2},$$

with initial conditions and boundary conditions. Notice that the glutamate-dependent source term in $P_0(k_1)$ is replaced by the ATP-dependent term $k_{\text{in}} B_{\max} A/(K_d+A)$ in P_i for $i \neq 0$. When Ca_i^{2+} waves are mediated only by the intracellular messenger (IP_3), we set $k_{\text{in}}=0$ in C(i) for $i \neq 0$.

On the other hand, ATP kinetics are defined domainwise in the extracellular space, $\Omega=\{\cup_i \bar{C}(i)\}\cup\{\text{Ex}\}$ with the boundary $\partial\Omega$ (Fig. 2), where $\bar{C}(i)$ is a domain right above C(i) in extracellular space and Ex is cell-free extracellular space. Notice that $\partial\Omega$ consists of four sides of the rectangular Ω in the realistic geometry [Fig. 2(b), while $\partial\Omega$ is found at both sides of the simplified geometry [Fig. 2(a)]. In $\bar{C}(i)$, with an extracellular volume dependent parameter γ, the equation of ATP kinetics (see Appendix B for more details) is

$$\frac{\partial A}{\partial t} = D_A \frac{\partial^2 A}{\partial x^2} - k_{-\text{ATP}} A + \gamma k_{\text{ATP}} \phi(P_i)(A_T - A), \tag{6}$$

where A_T is the intracellular concentration of ATP with the initial condition

$$A(x,0)=0.$$

The function ϕ describes ATP release kinetics either by hemichannels or by vesicular release. Because ϕ is unknown, we choose $\phi(P_i)=P_i/(\rho+P_i)$ for some constant ρ (Table I). It should be noted that a recent study[118] suggested that ϕ is a bell-shaped function of $[Ca_i^{2+}]$, but we assumed that ATP release is triggered by IP_3.[20,22]

On the other hand, for nonregenerative ATP release [Fig. 1(C2), (C4)], there is no source term in any but the glutamate-stimulated cell, and thus $k_{\text{ATP}}=0$ in Eq. (6) for $\bar{C}(i)$, $i \neq 0$. This applies in the cell-free region as well. In all cases, we use the boundary condition on $\partial\Omega$ as $D(\partial A/\partial n)=-A$ to reflect leakage of ATP to the surroundings [Fig. 2(c)].

For the numerical computations, Eqs. (2)–(6) in the domains in Fig. 2 were solved by the finite element method implemented by FEMLAB® with a choice of linear Lagrangian interpolation for the shape functions. The system of PDEs described on geometries defined in Fig. 2 was incorporated into FEMLAB and UMFPACK (Ref. 33) was chosen to solve the resulting nonsymmetric, sparse linear systems.

III. RESULTS AND DISCUSSION

A. Ca^{2+} wave propagation and evolution of Ca_i^{2+} response patterns in a network of cells

In a previous study it was demonstrated that the different Ca_i^{2+} response types are determined by $[IP_3]$, which, in turn, is controlled by the activities of PLC and PKC.[67] The effect of $[IP_3]$ on the complexity of calcium oscillations in a single cell was also addressed by Pittà *et al.*[88] in a simpler framework. Since IP_3 levels are different from one cell to another in an astrocytic network, we may expect different types of

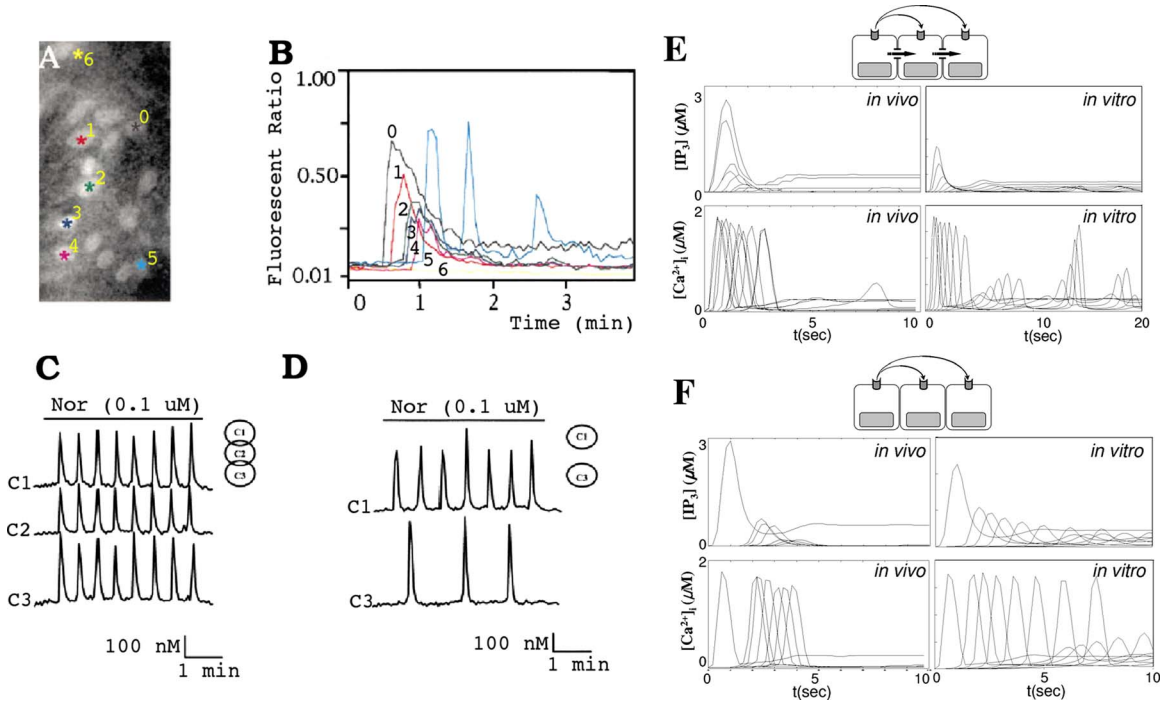

FIG. 3. (Color online) Evolution of the Ca_i^{2+} response types in cells. [(a) and (b)] Distribution and pattern of Ca_i^{2+} responses to focal application of receptor agonist in rat astrocytes in a 200×100 μm^2 rectangle (Ref. 113). [(c) and (d)] Noradrenaline-induced $[Ca_i^{2+}]$ oscillation in rat hepatocytes when three cells are connected and when the intermediate cell was excised (Ref. 111). [(e) and (f)] Simulation results from simplified geometry (*in vitro*) and realistic geometry (*in vivo*) corresponding to (a), (b) and (c), (d). The traces from left to right in (e) (*in vivo*) $[Ca_i^{2+}]$ correspond to C(i), i=0, 1, 3, 2, 9, 4, 8, 5, 7, 6, and 10 in descending order. The traces from left to right in (f) (*in vivo*) $[Ca_i^{2+}]$ correspond to $C(i)$, i=0, 2, 9, 1, 5, 8, and 4 with subthreshold Ca_i^{2+} responses in C(3) and C(10). The traces from top to bottom in (e) $[IP_3]$ correspond to C(i), i=1, 0, 2, 3, 9, 4, 8, 5, 7, 6, and 10 in descending order. Also, in (f), $[IP_3]$, the traces from top to bottom correspond to in C(i), i=0, 2, 9, 1, 5, 8, 4, 6, and 7 in descending order and $[IP_3]\simeq0$ in C(3) and C(10). In (e) (*in vitro*) and (f) (*in vitro*), the traces from top to bottom are $C(i), i=0, \pm1, \pm2, \ldots, \pm7$.

Ca_i^{2+} response in different cells. Indeed Venance *et al.*[113] reported an evolution of $[Ca_i^{2+}]$ response patterns in rat astrocytes [Figs. 3(a) and 3(b)]. In Figs. 3(a) and 3(b), cells 1–4 show a gradual change from a "transient with plateau-type" response pattern (cell 0) to a "transient without plateau-type" response pattern. Interestingly, the beginnings of a baseline spiking-type response pattern were observed in the fifth cell, whereas the sixth showed no response.

Another interesting observation was made by Tordjmann *et al.*,[111] who found that noradrenaline-induced $[Ca_i^{2+}]$ oscillation patterns in three interconnected rat hepatocytes were similar, whereas different Ca_i^{2+} patterns were observed in the first and third cells when those cells were physically separated by excising the intermediate second cell, thereby presumably removing direct coupling through gap junctions. Also, longer delays in the initial Ca_i^{2+} transients were observed in the latter case [Figs. 3(c) and 3(d)]. (Here one must be careful when Ca_i^{2+} dynamics in hepatocytes and astrocytes are compared because Ca_i^{2+} waves in hepatocytes are predominantly carried by IP_3 through intercellular gap junctions[111] while both intracellular IP_3 and extracellular messengers are believed equally importantly in Ca_i^{2+} waves in astrocytes.[53,25,27,26,54,44]

To determine whether the model can reproduce the results in Figs. 3(a)–3(d), Eqs. (2)–(6) were solved numerically on the geometries (Fig. 2) under the assumption of either only an intracellular messenger and nonregenerative extracellular messenger or only nonregenerative extracellular messenger [Fig. 1(C4), (C2)]. A sustained glutamate input (k_1) was used as a stimulus in both simplified and realistic geometries. For quantification, the values of $[Ca_i^{2+}]$ and $[IP_3]$ in the center of cell ($\star$ in Fig. 2) were calibrated in the realistic geometry, while the average values of $[Ca_i^{2+}]$ and IP_3 in cells were computed for the simplified geometry.

Figure 3(e) *in vivo* indicates that as the $[IP_3]$ level decreases from the stimulated cell [C(0)] to remote cells, the Ca_i^{2+} response patterns evolve from transient with plateau at C(0) to oscillations at C(9) and to baseline spiking at C(10), as reported in Ref. 67. Results for the model of an *in vitro* astrocytic network are similar, except that the amplitude of $[IP_3]$ is about half of that of *in vivo* model, because there are more gap junctions present in the *in vivo* model than in the *in vitro* model (Fig. 2).

Figures 3(c) and 3(d) can be understood in the same context in terms of $[IP_3]$. In the interconnected rat hepatocytes [Fig. 3(c)], there was almost no transition in Ca_i^{2+} response patterns from one cell to another, implying that the $[IP_3]$ levels in each cell are in a similar range or at least over some effective dosage (~0.1 μM) while quite different $[IP_3]$ levels are expected when the intermediate cell is excised and IP_3 diffusion is absent. The decrease level of $[IP_3]$ available in the third cell implies the transition from high to low frequency baseline spiking.[67] The longer delay in the initial Ca_i^{2+} spikes in Fig. 3(d) was also reproducible in both *in vivo* and *in vitro* model when gap junctional permeability

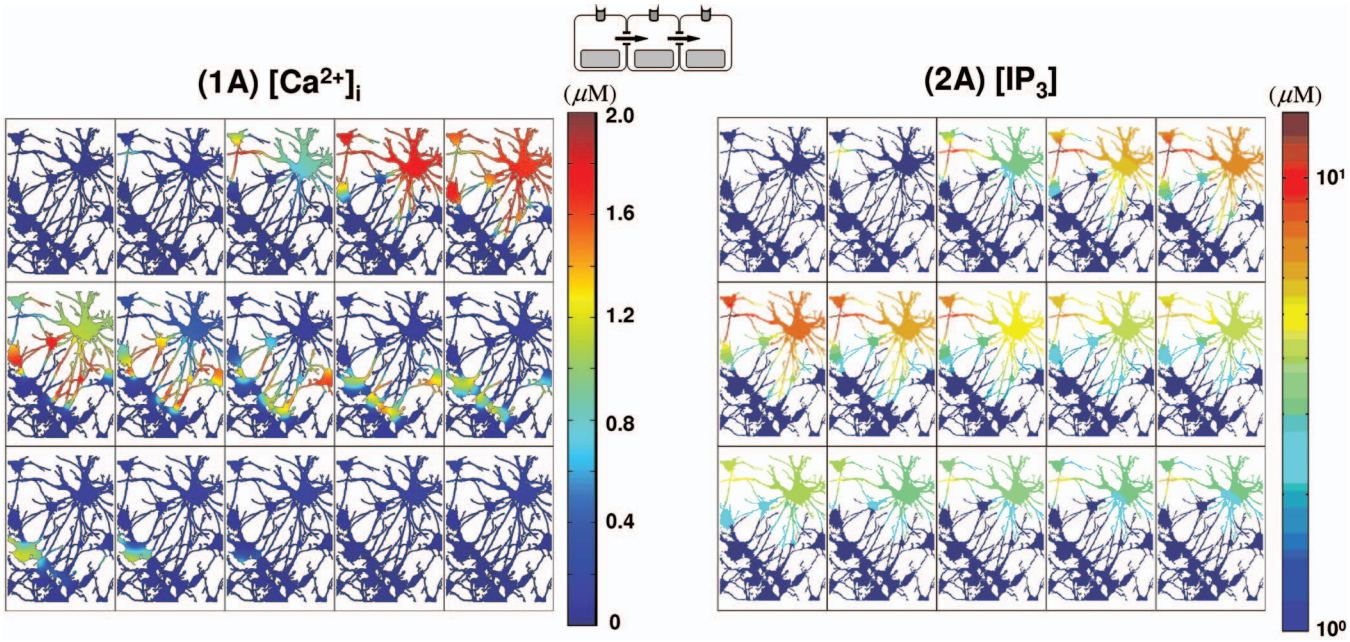

FIG. 4. (Color) Intracellular-messenger-mediated Ca_i^{2+} waves in a realistic network. (1A) Ca_i^{2+} waves by a glutamate stimulus in C(0) and mediated only by IP_3 diffusion are shown on a linear scale. (2A) The corresponding IP_3 waves plotted on a log scale. The temporal sequence of images in (1A) and (2A) runs from left to right and top to bottom. The elapsed time between images in (1A) and (2A) is $\Delta t=0.2$ s with a total time of 3 s ($t=0,0.2,0.4,\ldots,2.8,3$).

($k_{\text{perm }P}$) was set to zero, although the delay was more evident in the latter model [Figs. 3(e) and 3(f)].

B. Gap junction mediated versus P2YR mediated Ca_i^{2+} waves

In the absence of extracellular signaling, the distance that an initial calcium spike spreads depends on IP_3 diffusion. The threshold value of IP_3 for initiating a Ca_i^{2+} spike is ~0.1 μM (Figs. 4–6, Table II) and $[IP_3]$ decreases rapidly from one cell to the next as IP_3 diffuses through astrocytic gap junctions [Figs. 4(2A), 5(2A), and 6(2A), Table II]. As a result, the amplitudes of spikes along the spreading Ca_i^{2+} wave decrease rapidly and the wave dies within ~58.2 μm from C(0) [C(6), C(7), and C(10) in Fig. 4(1A), Table II] in the realistic geometry, whereas it vanishes in the fourth cell in the simplified geometry [Fig. 6(1A)]. Also, the velocity of Ca_i^{2+} waves decreases as shown in Figs. 5(1A) and 6(1A) and Table II.

On the other hand, when Ca_i^{2+} waves are mediated by nonregenerative ATP diffusion, $[IP_3]$ decreases more slowly than when the waves are mediated by IP_3 diffusion through gap junctions [Figs. 5(2B), 6(2B), and 7(2B), Table II]. Although the Ca_i^{2+} waves died after a few cells [Figs. 5(1B) and 6(1B), Table II] similar to the case of gap junction mediated Ca_i^{2+} waves, the amplitudes of initial spikes and the propagation velocity along Ca_i^{2+} wave remained constant [Figs. 5(1B) and 6(1B), Table II].

The effective dosage of ATP to trigger Ca_i^{2+} spike in the model was 3 μM [Figs. 5(3B) and 6(3B), Table II], which is similar to the value reported in the literature.[82,64] The velocity as measured by the spread of the peak of nonregenerative ATP wave spread was ~50 μm/s in the realistic geometry [Fig. 5(3B), Table II] and ~40 μm/s in the simplified geometry [4 cells in 1.5 s, Fig. 6(3B)], which is similar to reported values (41 μm/s; Ref. 82).

Another noticeable feature of Ca_i^{2+} waves by mediated by IP_3 diffusion is that there is very little delay in propagation between cells [Figs. 5(1A) and 6(1A), Table II], while Ca_i^{2+} waves by ATP signal show a longer delay time for propagation from one cell to the next [Figs. 5(1B) and 6(1B), Table II]. Although the diffusion coefficient of ATP is larger than that of IP_3 (Table I), the results in Figs. 5(1A), 5(2A), 6(1A), and 6(2A) illustrate the higher velocity of gap junction mediated Ca_i^{2+} waves compared to P2YR mediated waves. This difference stems from the fact that IP_3 is the critical species for initiating Ca_i^{2+} release, and when it spreads via gap junction there is little delay in initiating Ca_i^{2+} release, whereas additional time for IP_3 production is required for ATP signaling by P2YR. Because of this delay, P2YR mediated Ca_i^{2+} waves are expected to be slower than gap junction mediated waves, and this is borne out by the measured speeds: ~15 μm/s [Figs. 5(1B) and 6(1B), Table II] versus 40 μm/s [Figs. 5(1A) and 6(1A), Table II] in both simplified and realistic geometries. These also compare favorably to the experimentally observed ranges (15–27 $\mu m^2/s$; Refs. 15, 18, 82, 113, and 120). It has also been reported that in Ca_i^{2+} wave propagation from Muller cells into astrocytes, there was a considerable delay, 2.6 ± 0.2 s, while there was a shorter delay (0.85 s) in the case of wave spread from astrocyte processes to an adjacent Muller cell endfoot.[82] Other studies demonstrated a longer delay (5–10 s) in Ca_i^{2+} waves between different layers of cells in a hippocampal slice.[57] In the model, the delay times range between 0.4 and 1.6 s [Figs. 5(1B) and 6(1B), Table II].

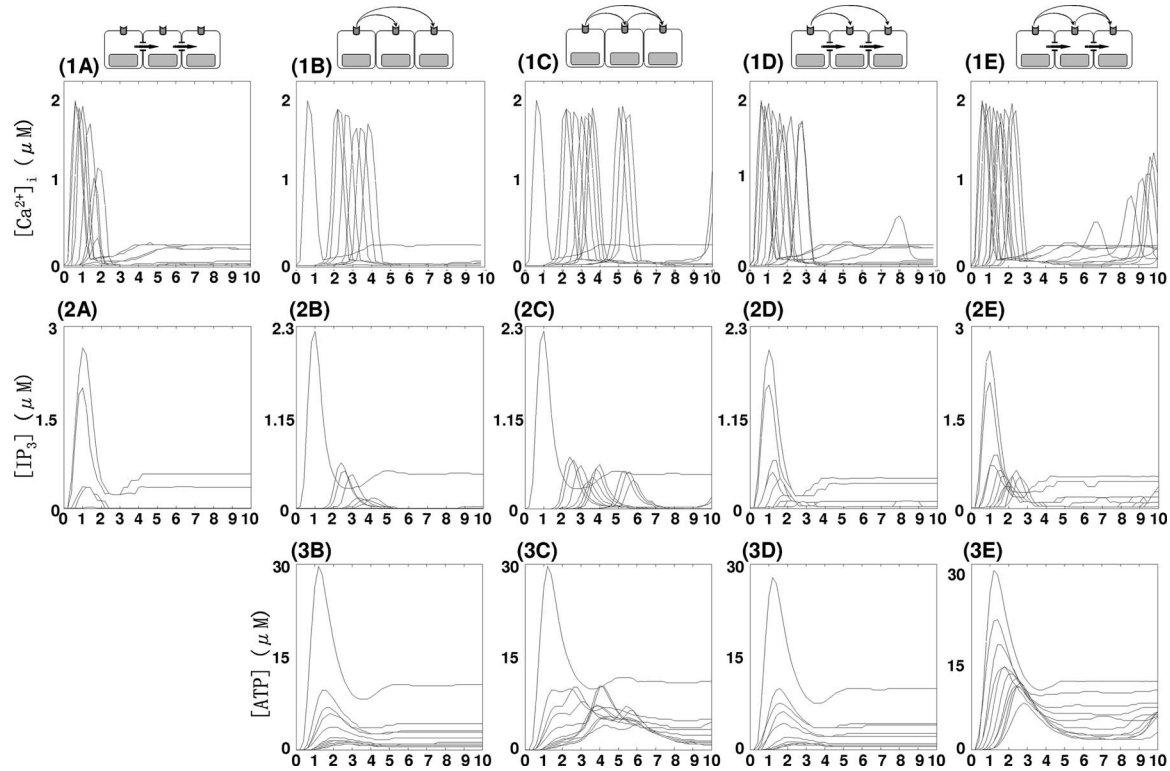

FIG. 5. A composite summary of the Ca_i^{2+} waves in the realistic cell network. Ca_i^{2+}, $[IP_3]$, and [ATP] in C(i) were measured at the locations marked as ⋆ in Fig. 2. The locations of the measuring point in descending order are C(2), C(9), C(1), C(3), C(4), C(8), C(5), C(10), C(7), and C(6) with distances from C(0) of 20.3, 29.8, 40.4, 42.4, 46.4, 49.3, 50.3, 58.2, 59.3, and 64.76 (μm). In (1A), the traces whose peaks are above 0.5 μM correspond to C(0), C(1), C(3), C(2), C(9), C(8), and C(4) from left to right, while the traces whose peaks are below 0.5 μM correspond to C(5) and C(7) from top to bottom. In (2A), the traces from top to bottom represent $[IP_3]$ in C(1), C(0), C(3), C(2), and C(10). In (1B), (1C), (2B), and (2C), the traces are of C(0), C(2), C(9), C(1), C(5), C(8), C(4), C(3), C(7), C(6), and C(10), while in distal order of C(0)-C(2)-C(9)-C(1)-C(5)-C(8)-C(4)-C(3)-C(7)-C(6)-C(10) from left top to bottom right traces in (3B) and (3C). In (1D) and (1E), the traces from left to right are Ca_i^{2+} from C(0), C(1), C(3), C(2), C(9), C(4), C(8), C(5), C(7), C(6) and C(10), whereas C(1)-C(0)-C(2)-C(3)-C(9)-C(4)-C(8)-C(7)-C(10) in (2D) and C(1)-C(0)-C(3)-C(2)-C(9)-C(4)-C(5)-C(8)-C(7)-C(6)-C(10) in (2E) from left top to bottom right. Finally, from left top to bottom right, C(0)-C(2)-C(1)-C(9)-C(3)-C(4)-C(8)-C(10)-C(7)-C(6) in (3D) and C(0)-C(1)-C(2)-C(3)-C(9)-C(4)-C(5)-C(8)-C(7)-C(6)-C(10) in (3E).

Another difference between P2YR and gap junction mediated Ca_i^{2+} waves *in vivo* is reflected in the local IP_3 concentration. Local $[IP_3]$ can be larger than 10 μM [Figs. 4(2A), 8(2D), and 8(2E)] for the *in vivo* gap junction mediated Ca_i^{2+} waves due to more "focused" diffusion along fine astrocytic processes. In contrast, the maximum $[IP_3]$ remains less than 3 μM for P2YR mediated waves [Figs. 7(2B) and 7(2C)]. On the other hand, in the simplified model which has more open connectivity in gap junctions, IP_3 concentrations are less than 3 μM in all cases, which is probably due to large gap junctional boundaries between cells (Fig. 6). A more detailed discussion on gap junctional connectivity and Ca_i^{2+} wave patterns can be found in Ref. 36.

C. The effects of regenerative ATP signaling

Another contentious issue in Ca_i^{2+} signaling is whether or not ATP signaling is regenerative.[37] To see how the regenerative of ATP release affects the Ca_i^{2+} waves, Eqs. (2)–(6) were solved either for $k_{ATP}=0$ or 0.184/s. The velocities of initial Ca_i^{2+} spikes under the two scenarios were not distinguishable, even though the distance of Ca_i^{2+} wave spread was larger for regenerative ATP [(1B) and (1C) in Figs. 5–7, Table II]. Other differences can be seen from the ATP and IP_3 profiles. When ATP release is assumed to be nonregenerative, peaks of [ATP] transients quickly decrease due to enzymatic degradation, whereas the summation of regenerative ATP release from each cell and diffusive spread from neighboring cells gives rise to steady amplitude of [ATP] transients in the regenerative case [Figs. 5(3B), 5(3C), 6(3B), and 6(3C)]. Although the waves travel further in the regenerative case, the ATP wave speed in both cases was ~40–50 μm/s [measured by the initial spikes in Figs. 5(3B), 5(3C), 6(3B), and 6(3C)].

Similar to what is observed for ATP wave propagation, in both cases the Ca_i^{2+} and IP_3 wave velocities are similar at ~40 μm/s [(1B), (1C), (2B), and (2C) in Figs. 5 and 6]. The peak IP_3 amplitude of the stimulated cell is unchanged at 2.3 μM but the peak IP_3 amplitudes of other cells diminish as a function of distance for nonregenerative ATP signaling, while they remain constant from the second cell on in the regenerative case due to ATP-stimulated IP_3 downstream of the stimulated cell [Figs. 5(2B), 5(2C), 6(2B), and 6(2C)]. Also, a slight decrease in the amplitude of Ca_i^{2+} transients was observed in the nonregenerative ATP mediated Ca_i^{2+} wave, but the amplitude of Ca_i^{2+} transients remains constant in the regenerative ATP mediated Ca_i^{2+} waves [Figs. 5(1B), 5(1C), 6(1B), and 6(1C)].

Given the variety of calcium responses including oscillations that exist in a single cell,[67] it is worthwhile to understand why there is no sustained wave propagation in a net-

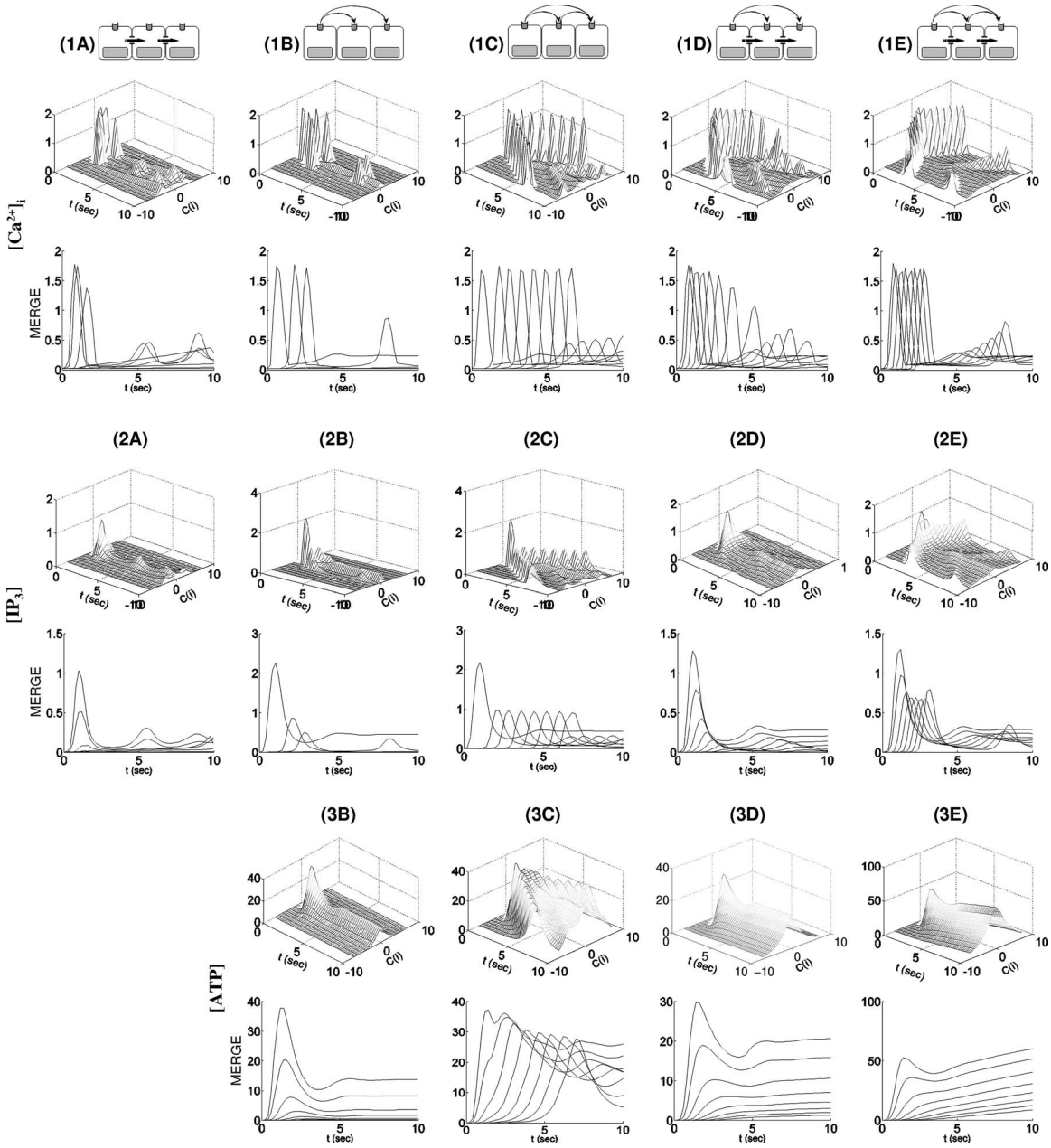

FIG. 6. Ca_i^{2+} waves in the simplified cell geometry. In the upper panels for Ca_i^{2+}, $[IP_3]$, and [ATP], the x- and y-axes represent time in seconds and the location of cells C(i) for $i=1,\ldots,10$, respectively. On the z-axis is shown the average of the quantity over the cell (i.e., the integral of the quantity divided by the cell volume) plotted in increments of $t=0.2$. The lower panels (MERGE) showed the projected traces from the upper panels onto the $y=0$ plane.

work. To this end we tested the linear stability of the steady state solution of Eq. (1) assuming zero gap-junctional permeability, which is equivalent to assuming that Ca_i^{2+} waves are mediated solely by ATP. The analysis of Eq. (1) shows that below the effective ATP dosage for Ca_i^{2+} response, all the real parts of the eigenvalues of Eq. (1) linearized about the steady state solution are negative, which prevents initiation of the Ca_i^{2+} response. Therefore, without regenerative ATP release the level of ATP that reaches the neighboring cells eventually drops below the effective ATP dosage as a result of diffusive spreading and enzymatic degradation (see Appendix C for details), and sustained propagation of Ca_i^{2+} waves is precluded. Furthermore, we have not found conditions that lead to propagation even if regenerative release is included.

D. Synergy of intra- and extracellular messengers

Thus far we have investigated the properties of Ca_i^{2+} response patterns initiated by either IP_3 or ATP alone. Now we consider cases when both intra- and nonregenerative extracellular messengers carry Ca_i^{2+} release signals. Because we assume nonregenerative ATP signaling, the intracellular dynamics other than in C(0) do not influence ATP evolution [Figs. 7(3B) and 8(3D)].

Recall that the time scale of direct IP_3 diffusion is faster than IP_3 generation via ATP signaling [Figs. 5(2A), 5(2B), 6(2A), and 6(2B)]. When both IP_3 and ATP are used for Ca_i^{2+} mobilization, IP_3 diffusion dominates Ca_i^{2+} wave initiation as far as the IP_3 concentration is above the effective threshold ($\sim 0.1\ \mu M$). Beyond that distance the generation of IP_3 via

TABLE II. The characteristics of Ca_i^{2+} waves mediated by IP_3 and/or ATP *in vivo* model.

		(A)	(B)	(C)	(D)	(E)
		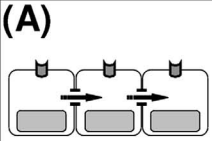	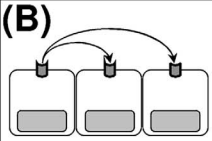	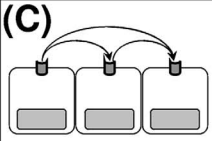	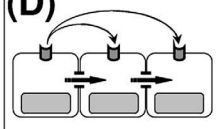	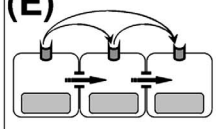
(1)$[Ca^{2+}]_i$	velocity (μm/s)	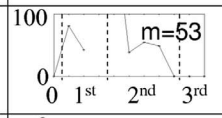 m=53	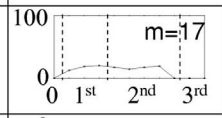 m=17	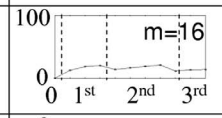 m=16	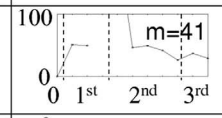 m=41	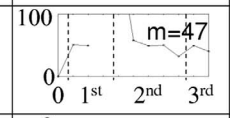 m=47
	delay (sec)	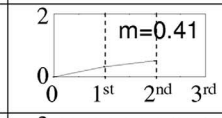 m=0.41	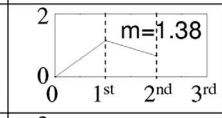 m=1.38	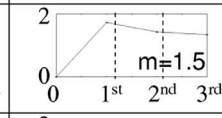 m=1.5	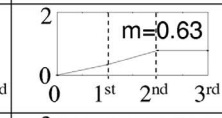 m=0.63	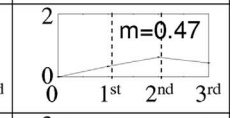 m=0.47
	amplitude (μM)	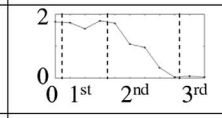	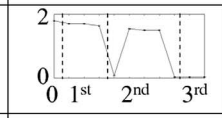	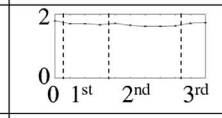	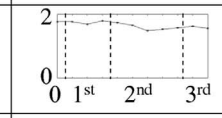	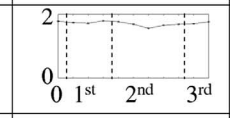
	distance (μm)	$C(0)\sim C(5)$ 50.3 μm	$C(0)\sim C(5)$ 50.3 μm	$C(0)\sim C(11)$ > 64.7 μm	$C(0)\sim C(11)$ > 64.7 μm	$C(0)\sim C(11)$ > 64.7 μm
(2)$[IP_3]$	velocity (μm/s)	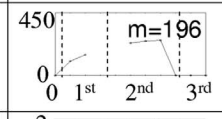 m=196	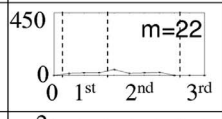 m=22	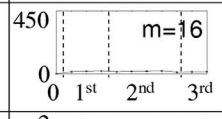 m=16	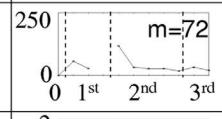 m=72	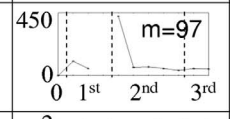 m=97
	delay (sec)	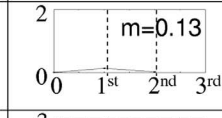 m=0.13	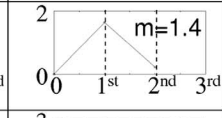 m=1.4	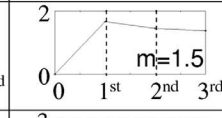 m=1.5	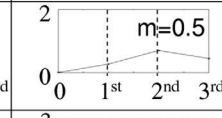 m=0.5	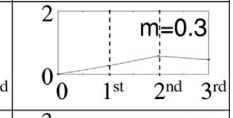 m=0.3
	amplitude (μM)	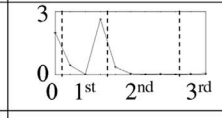	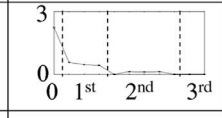	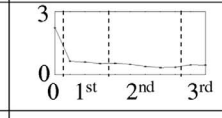	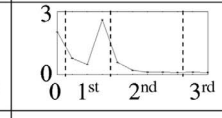	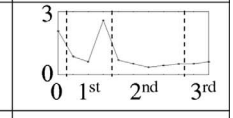
	distance (μm)	$C(0)\sim C(5)$ 50.3 μm	$C(0)\sim C(5)$ 50.3 μm	$C(0)\sim C(11)$ > 64.7 μm	$C(0)\sim C(11)$ > 64.7 μm	$C(0)\sim C(11)$ > 64.7 μm
(3)[ATP]	velocity (μm/s)	N/A	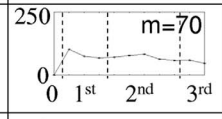 m=70	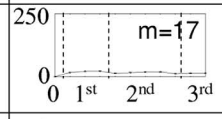 m=17	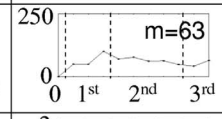 m=63	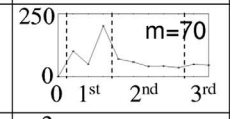 m=70
	delay (sec)	N/A	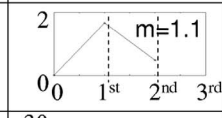 m=1.1	m=1.4	m=0.4	m=0.43
	amplitude (μM)	N/A				
	distance (μm)	N/A	$C(0)\sim C(5)$ 50.3 μm	$C(0)\sim C(11)$ > 64.7 μm	$C(0)\sim C(11)$ > 64.7 μm	$C(0)\sim C(11)$ > 64.7 μm

0: $C(0)$, 1st Colume ; [$C(2)$, $C(9)$, $C(1)$] , 2nd colume: [$C(3)$, $C(4)$, $C(8)$, $C(5)$, $C(10)$], 3rd colume: [$C(7)$, $C(6)$]

the ATP pathway serves to elevate IP_3 above the threshold. Therefore, in short range Ca_i^{2+} wave propagation by pure IP_3 diffusion is dominant, while Ca_i^{2+} wave propagation by ATP signaling is dominant in cells distant from the stimulation point [(1A), (1B), and (1D) in Figs. 5 and 6]. As the result, longer delay in Ca_i^{2+} wave propagation is observed for remote cell locations, in contrast with rapid continuous wave propagation near the stimulated cell [Figs. 5(1D) and 6(1D)].

Another consequence of synergy between intra- and extracellular messengers is the propagation distance. While either an ATP signal without IP_3 diffusion or IP_3 diffusion without an ATP signal results in decaying waves, the syner-

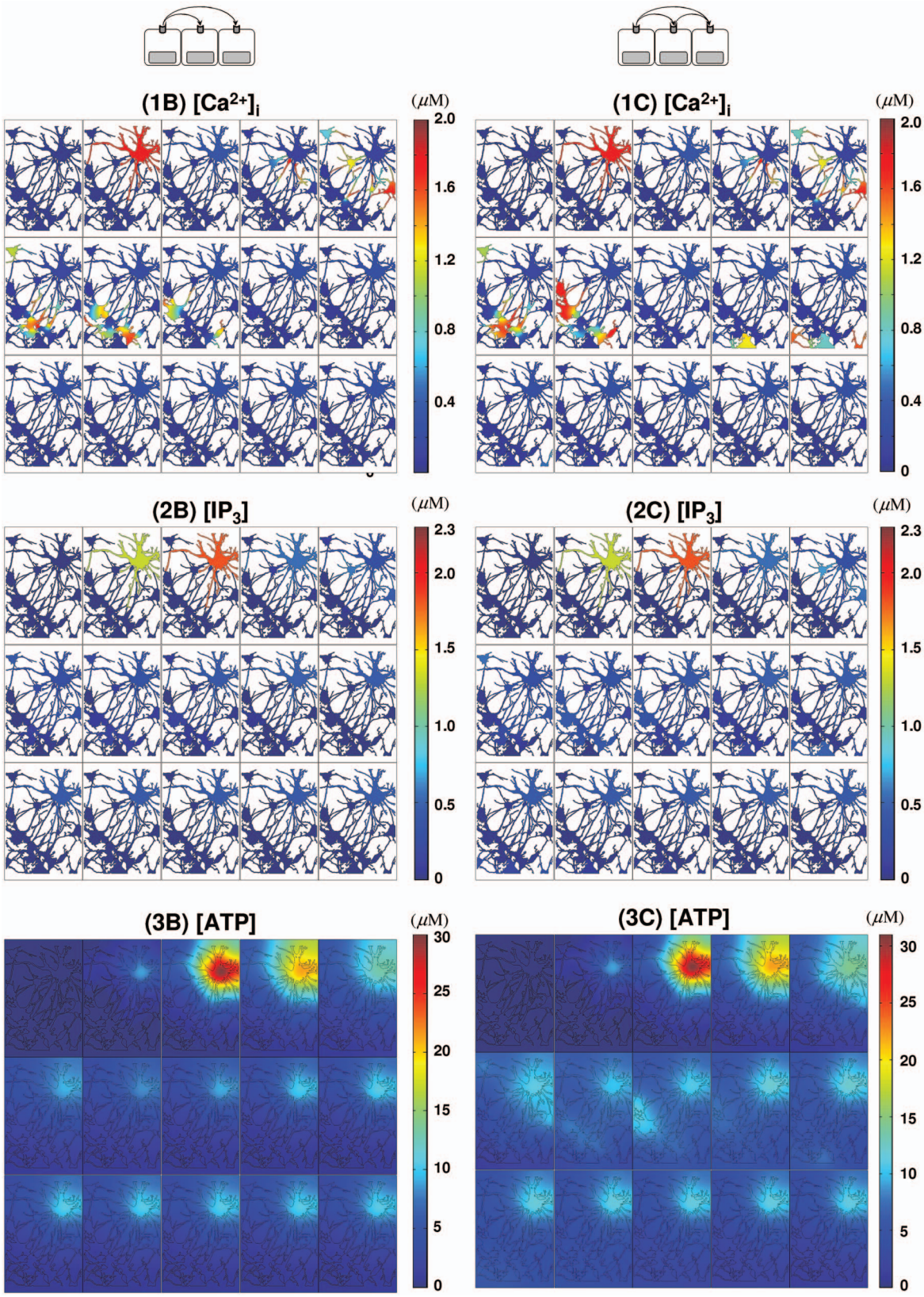

FIG. 7. (Color) Extracellular messenger mediated Ca_i^{2+} waves. Ca_i^{2+} waves initiated by a glutamate stimulus in C(0) and mediated only by ATP are shown. In (1B)–(3B), excitation is mediated by nonregenerative ATP spread, while regenerative ATP release is present in (1C)–(3C). The images in each panel [(1B)–(3B) and (1C)–(3C)] run from left to right and top to bottom. In each panel, the time elapsed between images is $\Delta t=0.6$ s with total time of 8.4 s ($t=0,0.6,1.2,\ldots,7.8,8.4$).

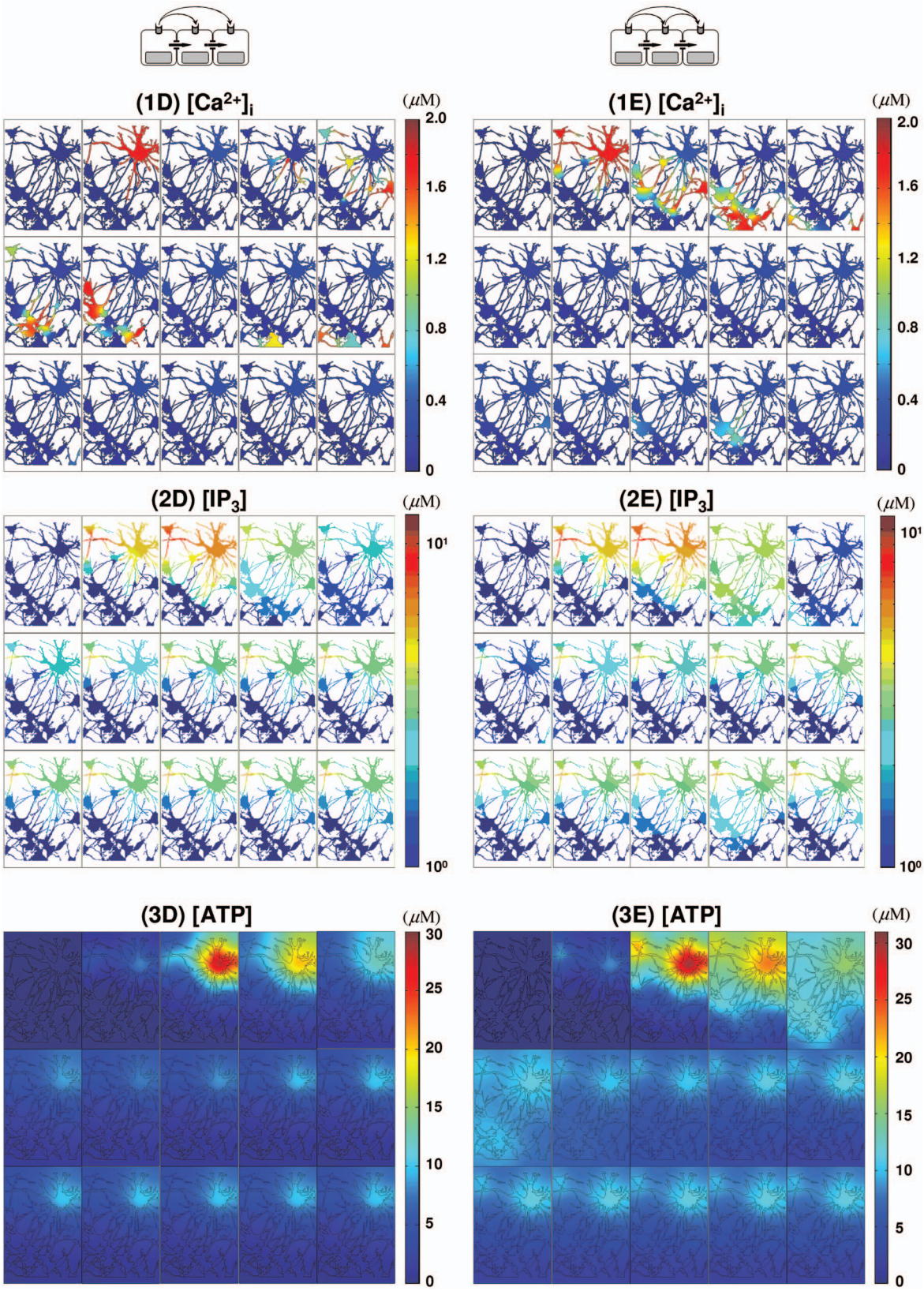

FIG. 8. (Color) Extracellular volume and Ca_i^{2+} wave by regenerative extracellular messenger

gistic activity of the two pathways gives rise to permanent waves that propagate through the entire computational domain, as shown in Figs. 4, 7, and 9. More quantitatively, (1A) and (2A) in Figs. 5 and 6 indicate that no Ca_i^{2+} responses were found in the distant cells [C(i), i=6, 7, 10 in the realistic geometry and $i \geq 4$ in the simplified geometry] when either intra- or extracellular messenger was applied independently. However, when both intra- and extracellular

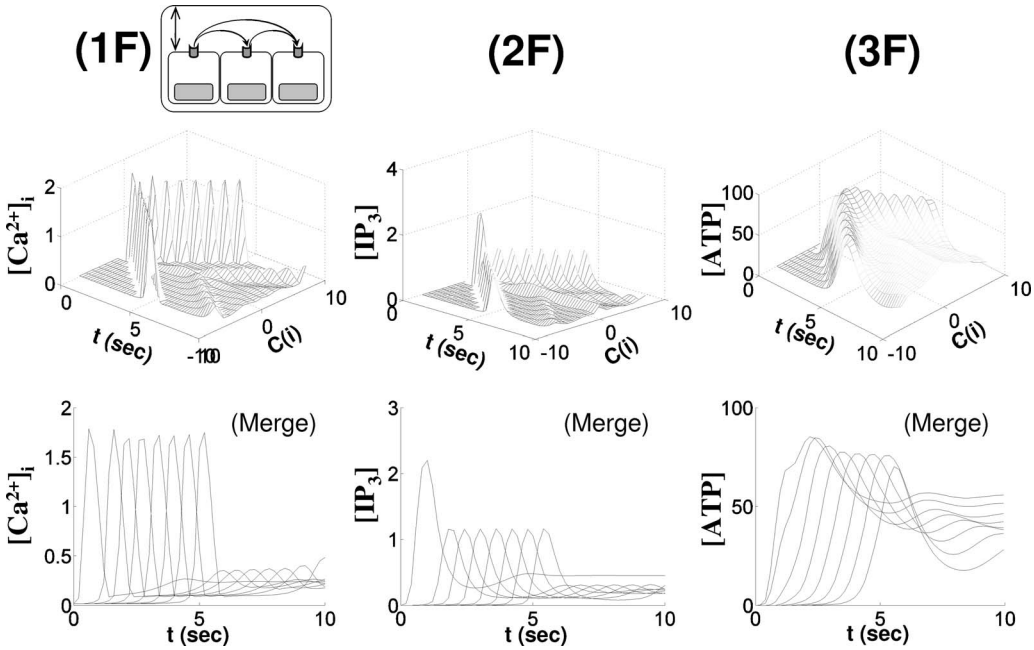

FIG. 9. The synergy between intra- and extracellular messengers in Ca_i^{2+} waves. Ca_i^{2+} waves initiated by glutamate in C(0) and mediated by both ATP and IP_3 are shown. In (1D)–(3D) are shown Ca_i^{2+} waves mediated by nonregenerative ATP spread, while regenerative ATP release is present in (1E)–(3E). The color maps for Ca_i^{2+} and ATP are on a linear scale [(1D), (3D), (1E), and (3E)], while IP_3 [(2D) and (2E)] is scaled logarithmically. The images in each panel [(1D)–(3D), (1E)–(3E)] are read from left to right and top to bottom and the time elapsed between images in each panel is $\Delta t=0.6$ s with total time of 8.4 s ($t=0,0.6,1.2,\ldots,7.8,8.4$).

messengers are present, Ca_i^{2+} transients are observed in all cells [Figs. 5(1D) and 6(1D), Table II]. This indicates that when both IP_3 and ATP are used for Ca_i^{2+} mobilization, the fast IP_3 diffusion can either mobilize Ca_i^{2+} or sensitize cells by eliciting a subthreshold Ca_i^{2+} responses. After additional IP_3 is received via the slower process of IP_3 production by ATP, the IP_3 level in sensitized cells reaches the threshold level ($\sim 0.1\ \mu M$) and Ca_i^{2+} transients are induced. As shown in (1B) and (2D) in Figs. 5 and 6, a slight decrease in the amplitude of Ca_i^{2+} transients was observed in the nonregenerative ATP mediated Ca_i^{2+} wave, while a constant amplitude of Ca_i^{2+} transients was observed in the regenerative ATP-mediated waves [Figs. 5(1C) and 6(1C)]. A similar observation can be made concerning ATP-mediated waves even with IP_3 diffusion through gap junctions. Moreover, regenerative ATP-mediated waves propagate like true traveling wave patterns, retaining the initial Ca_i^{2+} spike profile along the Ca_i^{2+} wave [Figs. 5(1C), 5(1E), 6(1C), and 6(1E)].

Another interesting result is that when IP_3 diffusion is included in the realistic geometry, a second wave was initiated from C(4) to C(9) which died out beyond C(9) [Figs. 5(1E) and 8(1E)]. In this case, C(2) shows a transient with plateau type of Ca_i^{2+} response pattern similar to that C(0) and C(1), while the cells C(4)$\cdots$C(9) show an oscillatory Ca_i^{2+} response pattern. Apparently the signal transferred from C(9) to its downstream neighbors was not strong enough to elevate IP_3 above threshold for wave initiation, but even so, the signal from C(9) integrated the signal relayed from C(4) and could, in living cells, influence the future response of these downstream cells [Figs. 5(1E) and 8(1E)].

In both the simplified and realistic geometries, the ATP wave propagation pattern indicates that for regenerative ATP without IP_3 diffusion, the peak amplitude of ATP was lower than for regenerative ATP with IP_3 diffusion [Figs. 5(3C), 5(3E), 6(3C), and 6(3E)]. Also, the maximum point of ATP spread from C(0) can be easily identified in Figs. 5(3C) and 6(3C), while when there is regenerative ATP with IP_3 diffusion, the extracellular effect of ATP released from a cell cannot be clearly identified [Figs. 5(3E) and 6(3E)]. Also, accumulation of ATP was observed in the simplified geometry due to the ATP released into the restricted extracellular space, something that is not observed in the sparsely distributed cells in the realistic geometry [Figs. 5(3E) and 6(3E)]. This may also explain why extracellular ATP is believed to be a major contributor to Ca_i^{2+} waves in cultured astrocytes.[54,58,11,53,63]

E. The role of the extracellular volume

In reality the extracellular space in the brain provides a tortuous path for molecular diffusion, and it is important to understand how the extracellular volume influences ATP signaling. For this purpose, the volume of the extracellular space was modified via an extracellular volume dependent parameter $\gamma=1/L$, where L is the thickness of the extracellular space (Appendix B). Here γ was chosen as $1.087\ \mu m^{-1}$, but because the ATP concentration in a cell is high ($30\ \mu M$), any change in L could result in a large change in ATP dynamics. To take this factor into account, we redid some computations in the case of regenerative ATP signaling using $\frac{1}{2}L=2\gamma$, which in effect doubles the source term $\gamma k_{\mathrm{ATP}}\phi(P)(A_T-A)$ in Eq. (6).

In comparison with Fig. 6(3C), the peak amplitude of ATP was doubled (from 38 to 85 μM), and the propagation

of ATP waves showed similar traveling wavelike patterns (Fig. 8). However, the average ATP and IP_3 wave velocity increased from 24.49 [Fig. 6(3C)] to 34.29 μm/s [Fig. 8(3F)]. The IP_3 profiles were not distinguishable between the two cases having similar amplitudes [Fig. 6(3C) and Fig. 8(3F)]. Similarly, Ca_i^{2+} wave velocity increased from 24.00 to 26.09 μm/s with constant amplitudes and the delay between cells was shortened [Fig. 6(3C) and Fig. 8(3F)]. Although the extracellular volume strongly influences the ATP dynamics, the effects on intracellular amplitudes of Ca_i^{2+} and IP_3 were minimal [Figs. 6(1C), 6(2C), 8(1F), and 8(2F)]. Thus the primary effect of the higher ATP signal is to speed up wave initiation and propagation.

In light of the nonuniform and complex spatial distribution of cells and extracellular space in the brain, these results imply that Ca_i^{2+} wave patterns can be very complex with a wide range of speeds and response times. Especially, when regenerative ATP is involved, the local maximal ATP that defines local Ca_i^{2+} wave velocity and delay time between cells was proportional to γ, and amplification and dilution of the strength of extracellular signaling could be accomplished by modifying the extracellular geometry. There is evidence that astrocytes have the ability to control the extracellular volume by gating VRACs and swelling in K^+ ion concentration and ATP dependent manner, even though the underlying mechanism has not been fully understood.[106,87,75,71,77] Therefore, ATP may have more complex, indirect, self-regulatory roles in diffusion by modulating volume-sensitive anion channels, which in turn affects ATP diffusion.

IV. CONCLUSIONS

It is widely believed that both direct coupling via the intracellular messenger IP_3 and indirect coupling via the extracellular messenger ATP are involved in cell-cell signaling in astrocyte networks, but the relative importance of each mode has not been established in general. The model developed herein, which utilizes a detailed model of signal transduction and intracellular calcium dynamics for single cells developed earlier,[67] allows for both modes of transport in both simplified and realistic network topologies. Simulations of the model in simplified and realistic geometries demonstrated that Ca_i^{2+} waves induced by individual messengers have distinct characteristics of propagation speed, propagation distance, delay between cells, and Ca_i^{2+} transient profiles. It was also found that synergistic effects of intracellular IP_3 and extracellular ATP on Ca_i^{2+} waves can be very complex, but the model developed here can be used to explore these effects.

While the IP_3-mediated Ca_i^{2+} waves propagate rapidly with at most a short delay between cells, they only propagate for a few cells and the corresponding amplitude of Ca_i^{2+} transients decreases significantly from cell to cell. Similar effects are observed for ATP-mediated waves, but the delay time in Ca_i^{2+} waves between cells is much longer for reasons adduced earlier, which leads to slower Ca_i^{2+} wave propagation and slower decay of Ca_i^{2+} transients.

Ca_i^{2+} waves mediated by both IP_3 and ATP display a mix of all the characteristics of the separate cases. While there is little or no delay in the Ca_i^{2+} wave close to stimulated cell, longer delays were observed in the remote cells. Overall decay of Ca_i^{2+} wave front transients was similar to that of ATP mediated Ca_i^{2+} wave, and Ca_i^{2+} wave propagation reached all the cells in the domain of consideration.

When regenerative ATP release was considered, the Ca_i^{2+} waves display a more permanent form and propagate at a constant speed, regardless of whether or not IP_3 served as a messenger. However, the wave speed was much larger when both IP_3 and regenerative ATP were involved [Fig. 7(1C), (1E)]. The characteristics of Ca_i^{2+} waves in this case are summarized in Table II. One clear conclusion is that regenerative release of ATP can lead to long distance propagation in networks.

While the qualitative behaviors of Ca_i^{2+} responses are independent of the geometries considered, IP_3 kinetics strongly depend on the geometries especially on the gap junctional connectivity among the astrocytes. When higher gap junctional connectivity was established through an astrocytic network, IP_3 easily diffuses out to neighboring cells, thereby controlling the $[IP_3]$ in cells. In contrast, the lower gap junctional connectivity observed in the realistic geometry of an astrocyte network leads to local $[IP_3]$ greater than 10 μM.

Regenerative ATP-driven waves also show geometry dependence. When cell density in the astrocytic network is high as in the case of the simplified geometry, regenerative ATP along can exceed the ATP decay rate and lead to local elevated concentrations for the parameters chosen. However, in the realistic geometry where there is a large area of cell free domains, the ATP released decays rapidly and the concentration remains close to the steady state level. Of course no geometry dependency in observed ATP is nonregenerative because the only ATP release is from the stimulated cell.

Experimentally observed Ca_i^{2+} waves in astrocyte networks exhibit decaying speeds (from the site of initiation) in the range of 200 μm,[15,113] a maximal propagation range of 200–350 μm in radius, and a maximal speed of 15–27 μm/s.[15,113,120,82,18] Our results replicate the decaying amplitudes when Ca_i^{2+} waves are mediated by either IP_3 or IP_3 and nonregenerative ATP, and the decrease in the velocity is observed in both cases. The maximal velocity in both cases is over 40 μm/s, which is larger than the values reported in the literature. However, when IP_3 was the only messenger, the effective range of Ca_i^{2+} waves was much lower than 200–350 μm, while Ca_i^{2+} waves propagate over 100 μm. In contrast, when regenerative ATP release is involved the waves display a more permanent form, which has not been reported. From this we conclude that Ca_i^{2+} waves in an astrocyte network are probably mediated by both intracellular IP_3 and nonregenerative extracellular ATP (or partially regenerative ATP as suggested in Ref. 74).

ACKNOWLEDGMENTS

This work was supported by NIH Grant GM 29123 (Hans G. Othmer) and NIH RO1 GM073846 (Anne K. Kenworthy).

APPENDIX A: PHYSICAL INTERPRETATION OF SIMPLIFIED TEMPORAL MODEL

Examination of Eq. (1) indicates that each equation has a source term and a decay term. For example,

$$\frac{dP}{dt} = J^P_{\text{source}} - J^P_{\text{decay}},$$

where $J_{\text{source}}=k_1C/(1+k_2K)$ and $J_{\text{decay}}=k_3P$. Therefore IP_3 production by PLC (J_{source}) is a function of cytosolic free Ca_i^{2+} and PKC with property $J_{\text{source}} \propto C$, $1/K$ with dependence on some parameters $k_1(s^{-1})$ and $k_2(\mu M^{-1})$. Since K is positive and the denominator $(1+k_2K) \geq 1$, the expression shows explicit inhibition of PKC in IP_3 production. Likewise, the activation of PKC shows the relationships PKC $\propto Ca_i^{2+}$ and free PKC (K_0-K) and

$$\frac{dK}{dt} = J^K_{\text{activate}} - J^K_{\text{decay}},$$

where $J_{\text{activate}}=k_4C(K_0-K)$ and $J_{\text{decay}}=-k_5K$. Here, $k_4(\mu M^{-1}\ s^{-1})$ is the rate constant for K and C binding and k_5 is decay rate for K.

Although in R-kinetics, the source term is quite complicated comparing with previous two cases, we can apply similar argument. Previously, the Tang and Othmer[107] Ca^{2+} model was implemented for IP_3 induced Ca^{2+} release from the ER,

$$IP_3R \overset{IP_3}{\rightleftharpoons} IP_3 \cdot IP_3R \overset{Ca^{2+}}{\rightleftharpoons} Ca^{2+} \cdot IP_3 \cdot IP_3R$$

$$\overset{Ca^{2+}}{\rightleftharpoons} Ca^{2+} \cdot Ca^{2+} \cdot IP_3 \cdot IP_3R,$$

where R $(Ca^{2+} \cdot Ca^{2+} \cdot IP_3 \cdot IP_3R) \propto P$, C^2, and free IP_3R. This leads us to

$$\frac{dR}{dt} = J^R_{\text{activate}} - J^R_{\text{decay}}$$

for activated state ($J_{\text{activate}} \propto PC^2IP_3R$) and decay ($J_{\text{decay}} \propto R$) of R. Because we want an ODE system of P, K, R, and C, we followed the computation described in Refs. 107 and 66 to remove the dependency on free IP_3R of J_{activate}. This step leads us to $J^R_{\text{activate}}=k_6PC^2(R_T-R)/1+k_7P(1+k_8C)$ and $J^R_{\text{decay}}=k_9R$ as desired, where $k_6(\mu M^{-2}\ s^{-1})$ is the binding rate constant for P, C^2, and IP_3R, $k_9(s^{-1})$ is the offrate constant of R, $k_7(\mu M^{-1})$, and $k_8(\mu M^{-1})$ are the affinity constant for (IP_3, IP_3R) and (Ca_i^{2+}, $IP_3 \cdot IP_3R$).

Finally, the cytosolic Ca_i^{2+} dynamics is governed by following equation:

$$\frac{dC}{dt} = J^C_{\text{leak}} + J^C_{IP_3} - J^C_{\text{SERCA}},$$

where J^C_{leak} is the basal Ca_i^{2+} release from ER, $J^C_{IP_3}$ is the IP_3 induced Ca_i^{2+} release, and J^C_{SERCA} is the clearance of Ca_i^{2+} by SERCA pump on ER. If we let k_c (micromolar) be volume averaged Ca_i^{2+} concentration in cytosol (i.e., the equilibrium of Ca_i^{2+} levels the cytosolic Ca_i^{2+} concentration approach when the whole ER network is ruptured), then

$$J_{\text{leak}} = k_{10}(k_c - C),$$

where $k_{10}(s^{-1})$ is the basal Ca_i^{2+} release rate. The IP_3 induced Ca^{2+} release ($J^C_{IP_3}$) is a function of (k_c-C) and $Ca^{2+} \cdot IP_3 \cdot IP_3R$ (i.e., $J_{IP_3} \propto (k_c-C)[Ca^{2+} \cdot IP_3 \cdot IP_3R]$), but if we use the similar argument to express $Ca^{2+} \cdot IP_3 \cdot IP_3R$ in term of R as we used in free IP_3R (Refs. 107 and 66) to get

$$J_{IP_3} = \bar{k}_{11}\frac{\tilde{k}_{11}CP(R_T-R)}{1+k_7P(1+k_8C)}(k_c - C),$$

where $\tilde{k}_{11}(\mu M^{-2})$ denotes affinity constant for C, P, and free IP_3R binding, and $\bar{k}_{11}(\mu M^{-1}\ \text{sec}^{-1})$ denotes Ca^{2+} release rate from IP_3R $Ca^{2+}Ca^{2+}$ channels. If we define $k_{11}(\mu M^{-3}) = \bar{k}_{11}\tilde{k}_{11}/k_{10}$, then we can combine J^C_{leak} and $J^C_{IP_3}$ as J^C_{source},

$$J^C_{\text{source}} = J^C_{\text{leak}} + J^C_{IP_3} = k_{10}\left(1 + \frac{k_{11}PC(R_T-R)}{1+k_7P(+k_8C)}\right)(k_c - C).$$

Finally, we assume that J_{SERCA} follows the Hill-type kinetics with Hill coefficient two[67] so that

$$J_{\text{SERCA}} = \frac{k_{12}C^2}{C^2+k_{p2}^2},$$

where $k_{12}(\mu M\ s^{-1})$ and $k_{p2}(\mu M)$ denote the maximal Ca^{2+} pumping rate and Ca^{2+} sensitivity of the SERCA pump, respectively.

APPENDIX B: ATP KINETICS

Let the height of extracellular space at the location of ATP release be L and define M as total mass of ATP (A) in the infinitesimal volume at the ATP release site (i.e., $M=AL\delta x\delta y$). From the conservation of mass and ATP decay by enzyme, the change in M over time is given by

$$\frac{\partial M}{\partial t} = \Sigma \dot{m}_{\text{in}} - \Sigma \dot{m}_{\text{out}} - \dot{m}_{\text{decay}}, \tag{B1}$$

where $\dot{m}_{\text{in}}=q_{x,\text{in}}\delta yL+q_{y,\text{in}}\delta xL+q_{z,\text{in}}\delta x\delta y$ and $\dot{m}_{\text{out}}=q_{x,\text{out}}\delta yL+q_{y,\text{out}}\delta xL$ denote mass fluxes while $\dot{m}_{\text{decay}}=k_{-\text{ATP}}M$ represents loss of mass due to decay.

Assuming Fick's law diffusion for the fluxes, applying a Taylor series expansion, and truncating, we obtain

$$\frac{\partial A}{\partial t} = -D_A\Delta A - \frac{1}{L}q_{z,\text{in}} - k_{-\text{ATP}}A, \tag{B2}$$

which does not involve z.

If the extracellular space is assumed to be uniform in height L, the value of L is computed from the observation that body fluid is composed of 28.0 l of intracellular fluid and 14.0 l of extracellular fluid, which is again composed of 3.0 l plasma fluid and 11.0 l of interstitial fluid. From the ratio of interstitial and intracellular fluids of 11/28,[55] we have $L=0.4l(\mu m)$, where l is the thickness of cells. With a choice of $l=2.33$, the cell thickness, we estimated $L=0.92$ μm (Table I, Fig. 2).

Because the ATP release mechanism is unknown, we assume that ATP release is proportional to the ATP concentration gradient between intra- and extracellular spaces in IP_3 dependent manner,

$$q_{z,\mathrm{in}} = k_{\mathrm{ATP}}\phi(P)(A_T - A),$$

where $k_{\mathrm{ATP}}(\mathrm{s}^{-1})$ is the ATP release rate, $\phi(P)$ is the IP_3 dependence of ATP release, and A_T is the intracellular concentration of ATP. The dependence of ATP release on IP_3 has been reported from some studies,[19,20] but the function ϕ is unknown and we will choose $\phi(P_1)=P_1/(\rho+P_1)$ in the current model. We will approximate $k_{\mathrm{ATP}}(\mathrm{s}^{-1})$ so that the peak amplitude of ATP release is 30 μM.

Putting this and Eq. (B2) together, we get

$$\frac{\partial A}{\partial t} = D_A \Delta A + \frac{1}{L} k_{\mathrm{ATP}} f(P)(A_T - A) - k_{-\mathrm{ATP}} A. \tag{B3}$$

In summary, the ATP kinetics can be described domainwise as the initial boundary value problem

$$\frac{\partial A}{\partial t} = \begin{cases} D_A \dfrac{\partial^2 A}{\partial x^2} + \gamma k_{\mathrm{ATP}} f(P_1)(A_I - A) - k_{-\mathrm{ATP}} A \\ \quad \text{in } C(i)(0,\infty) \\ D_A \dfrac{\partial^2 A}{\partial x^2} + - k_{-\mathrm{ATP}} A \quad \text{in } \mathrm{Ex}(0,\infty), \end{cases}$$

$$A(x,y,0) = 0, \quad D_A \frac{\partial A}{\partial n} = -A \quad \text{on } \Omega,$$

where $i=0,\ldots,10$ and $\gamma=1/L$. For nonregenerative ATP release, we set $k_{\mathrm{ATP}}=0$.

APPENDIX C: CA_i^{2+} WAVE PROPAGATION

Since we are interested in P2YR mediated Ca_i^{2+} waves, we assume that $k_{\mathrm{perm}\ P}=0$ in this section. A necessary condition for a Ca_i^{2+} wave initiated in one astrocyte to propagate to neighboring astrocytes is that $[IP_3]$ in the neighboring astrocytes should be above the effective dosage for Ca_i^{2+} response. Our previous study[67] indicates that various Ca_i^{2+} responses may occur for $[IP_3]$ above the effective dosage via a change in the linear stability of the steady state solution. If $[IP_3]$ is not high enough then the steady state solution remains stable and there exists no Ca_i^{2+} response in the cell, i.e., a Ca_i^{2+} wave stops. In this sense, Ca_i^{2+} wave propagation in an astrocytic network is completely determined by the linear stability of the steady state solution to Eq. (1),

$$\begin{aligned} \frac{dR}{dt} &= \frac{k_6 P C^2 (R_T - R)}{1 + k_7 P (1 + k_8 C)} - k_9 R, \\ \frac{dC}{dt} &= k_{10}\left(1 + \frac{k_{11} P C (R_T - R)}{1 + k_7 P (1 + k_8 C)}\right)(k_c - C) - \frac{k_{12} C^2}{C^2 + k_{p2}^2}, \end{aligned} \tag{C1}$$

which was studied extensively in Ref. 107 for $K=0$. Let $P=\tilde{P}$, which is above the effective dosage such that linearized Eq. (C1) at the steady state solution has a pair of complex conjugate eigenvalues. By a continuity argument applied to the eigenvalues, we can prove that there exists an open set around $(\tilde{P},0)$ where the linearized equation (C1) at the steady state solution has complex conjugate eigenvalues.

Next, If we write Eq. (1) as $dX/dt=\Phi(X)$, where $X=(P,K,R,C)$, the steady state solutions $\bar{X}=(\bar{P},\bar{K},\bar{R},\bar{C})$ of Eq. (1) are given by $\Phi(\bar{X})=0$. Linearizing about $\bar{X}$, we get

$$\frac{d(X-\bar{X})}{dt} = D\Phi(\bar{X})(X-\bar{X}), \tag{C2}$$

and the linear stability of $\bar{X}$ is determined by the eigenvalues $\Lambda=(\mu_1,\mu_2,\lambda_1,\lambda_2)$ of the matrix $D\Phi(\bar{X})$. Because there exists an open set around $(\tilde{P},0)$ where linearized Eq. (C1) at the steady state solution has complex conjugate eigenvalues, if P and K dynamics are confined in the open set around $(\tilde{P},0)$, Eq. (C2) also has complex conjugate eigenvalues. Indeed, we can find an invariant rectangular domain near $(\tilde{P},0)$ bounded by

$$P = \frac{k_1 \bar{C}(k_4 \bar{C} + k_5)}{k_3(k_4(k_2 K_T + 1)\bar{C} + k_5)} + \epsilon,$$

$$P = \frac{k_1 \bar{C}(k_4 \bar{C} + k_5)}{k_3(k_4(k_2 K_T + 1)\bar{C} + k_5)} - \epsilon,$$

$$K = \frac{K_T \bar{C}}{\dfrac{k_5}{k_4} + \bar{C}} + \epsilon, \quad K = \frac{K_T \bar{C}}{\dfrac{k_5}{k_4} + \bar{C}} - \epsilon.$$

To see this, we explicitly compute $\bar{X}=(\bar{P},\bar{K},\bar{R},\bar{C})$ by solving the following algebraic equations:

$$0 = \frac{k_1 \bar{C}}{(1 + k_2 \bar{K})} - k_3 \bar{P}, \tag{C3}$$

$$0 = k_4 \bar{C}(K_T - \bar{K}) - k_5 \bar{K}, \tag{C4}$$

$$0 = \frac{k_6 \bar{P} \bar{C}^2 (R_T - \bar{R})}{1 + k_7 \bar{P}(1 + k_8 \bar{C})} - k_9 \bar{R}, \tag{C5}$$

$$0 = k_{10}\left(1 + \frac{k_{11} \bar{P} \bar{C} (R_T - \bar{R})}{1 + k_7 \bar{P}(1 + k_8 \bar{C})}\right)(k_c - \bar{C}) - \frac{k_{12} \bar{C}^2}{\bar{C}^2 + k_{p2}^2}. \tag{C6}$$

Beginning with Eq. (C4), by solving for $\bar{K}$,

$$\bar{K} = \frac{K_T \bar{C}}{\dfrac{k_5}{k_4} + \bar{C}}. \tag{C7}$$

This implies that the steady state of PKC follows sigmoidal or hyperbolic dose-response curve in $\bar{C}$ in which the binding of a ligand to a single binding site is completely defined by the concentration of the binding site ($B_{\max}=K_T$) and the concentration of unbound ligand at which the binding site is 50% occupied [the equilibrium dissociation constant ($K_d=k_5/k_4$)]. Equation (C7) further indicates that

$(dK/dt)<0$ on $K=K_T\bar{C}/(k_5/k_4+\bar{C})+\epsilon$ and $(dK/dt)>0$ on $K=K_T\bar{C}/(k_5/k_4+\bar{C})-\epsilon$. Substituting Eq. (C7) into Eq. (C3), we also get

$$\bar{P}=\frac{k_1\bar{C}}{k_3(1+k_2\bar{K})}=\frac{k_1\bar{C}(k_4\bar{C}+k_5)}{k_3(k_4(k_2K_T+1)\bar{C}+k_5)}, \tag{C8}$$

which implies that $(dP/dt)<0$ on $P=k_1\bar{C}(k_4\bar{C}+k_5)/[k_3(k_4(k_2K_T+1)\bar{C}+k_5)]+\epsilon$ and $(dP/dt)>0$ on $P=k_1\bar{C}(k_4\bar{C}+k_5)/[k_3(k_4(k_2K_T+1)\bar{C}+k_5)]-\epsilon$. Note that Eqs. (C7) and (C8) indicate that $\bar{K}\simeq\bar{C}\ll 1$ (even $\bar{K}\simeq 0$ for some k_5/k_4) and $\bar{P}\sim(k_1/k_3)\bar{C}+O(\bar{C}^2)$ for $\bar{C}\ll 1$, or $\bar{P}$ as a function of k_1/k_3 (i.e., $\bar{P}\simeq\tilde{P}$ for some k_1/k_3). Because ϵ is an arbitrarily small positive number, we may assume that the invariant domain is a proper subset of the open set in which Eq. (C1) is oscillatory. This result further indicates that the steady state $(\bar{P},\bar{K})$ is stable (the real parts of associated eigenvalues are negative), ruling out the existence of any periodic orbit.

We further represent nullclines of C and R explicitly. By using Eq. (C8), from Eq. (C5),

$$f(\bar{C},\bar{R})\equiv\frac{k_6PC^2(R_T-R)}{1+k_7P(1+k_8C)}-k_9R=0,$$

$$\bar{R}=\frac{k_6R_T\bar{P}\bar{C}}{k_9(1+k_7\bar{P}(1+k_8\bar{C}))+k_6\bar{P}\bar{C}}=\frac{k_6k_1R_T\bar{C}^2(k_4\bar{C}+k_5)}{k_9(k_3(k_4(k_2K_0+1)\bar{C}+k_5)+k_7k_1\bar{C}(k_4\bar{C}+k_5)(1+k_8\bar{C}))+k_6k_1\bar{C}^2(k_4\bar{C}+k_5)}, \tag{C9}$$

which is a sigmoidal curve in C. Note that $\bar{R}$ can be regarded as a function of k_1/k_2 if we divide both denominator and numerator by k_1. Finally to get $\bar{C}$, if we rewrite Eq. (C6), as

$$g(\bar{C},\bar{R})\equiv k_{10}\left(1+\frac{k_9k_{11}}{k_6}\bar{R}\right)(k_c-\bar{C})-\frac{k_{12}\bar{C}^2}{\bar{C}^2+k_{p2}^2}=0. \tag{C10}$$

Equations (C9) and (C10) provide explicit expressions for $\bar{C}$ versus $\bar{R}$ so that we can plot the nullclines, $dC/dt=0$ and $dR/dt=0$. For the C nullcline, if we solve Eq. (C10) for $\bar{R}$, then

$$\bar{R}=\frac{k_6}{k_9k_{11}}\left(\frac{k_{12}C^2}{k_{10}(k_c-C)(C^2+k_{p2}^2)}-1\right),$$

$$g(\bar{C},\bar{R})\equiv\bar{R}-\frac{k_6}{k_9k_{11}}\left(\frac{k_{12}C^2}{k_{10}(k_c-C)(C^2+k_{p2}^2)}-1\right). \tag{C11}$$

So far, it was shown that $R-C$ system in Eq. (1) can have complex conjugate eigenvalues. Also, the nullclines of Eq. (1) can be reduced into manifolds in $\bar{R}-\bar{C}$ space. By studying the local behavior of the $R-C$ nullclines $f(C,R)=0$ and $g(C,R)=0$ at a steady state $\bar{X}$, we provide a condition for Ca_i^{2+} wave propagations in terms of $k_1(A)$.

Since the right-hand side of Eq. (C11) is independent of k_1 as we can see from Figs. 10(a)–10(d), C nullcline $(g(C,R)=0)$ does not change as k_1 varies. Only R nullcline $[f(C,R)=0]$ changes, i.e., $\bar{R}$ nullcline moves upward changing its curvature (and eigenvalues) as k_1 (PLC activity) increases. Also, for $\bar{X}=(\bar{C},\bar{R})$, both $\bar{R}$ and $\bar{C}$ increase as k_1 increases.

Consider now Fig. 10(e). If the complex conjugate eigenvalues λ_1 and λ_2 are associated with $\bar{X}$, λ_i, $i=1,2$ satisfy

$$0=|A-\lambda_iI|, A=\begin{bmatrix}\frac{\partial f}{\partial C} & \frac{\partial f}{\partial R}\\ \frac{\partial g}{\partial C} & \frac{\partial g}{\partial R}\end{bmatrix}.$$

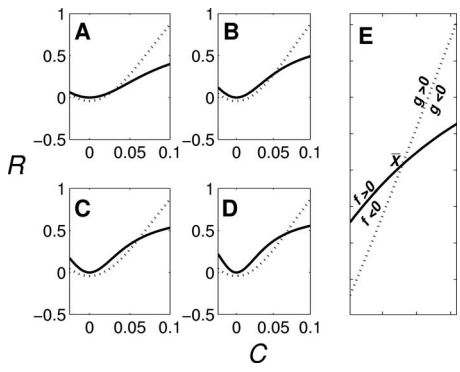

FIG. 10. Nullclines of C and R as k_1 varies C nullcline $[g(C,R)=0$: dotted line] and R nullcline $[f(C,R)=0$: solid line]. [(a)–(d)] $C-R$ nullclines for $k_1=0.5$, 1, 1.5, and 2. (e) $C-R$ nullclines near the steady state point $(\bar{X})$.

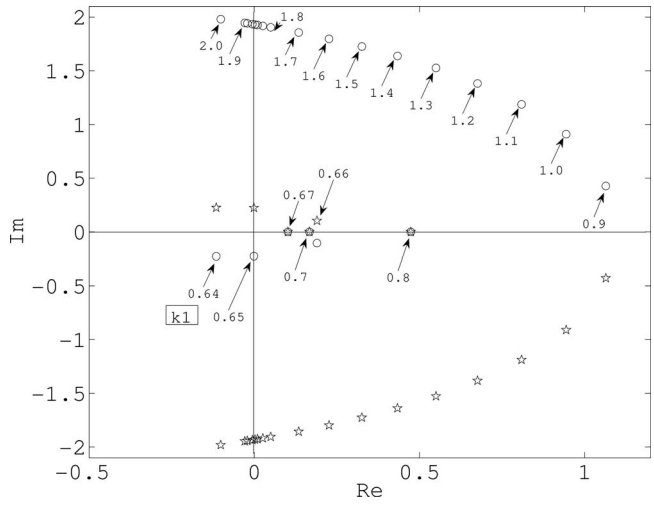

FIG. 11. Conjugate complex eigenvalues.

At the steady state $\bar{X}$, $\partial f/\partial C<0$, $\partial f/\partial R>0$, and $\partial g/\partial C<0$, $\partial g/\partial R>0$, which indicates that the sign of $\mathrm{tr}\, A=\lambda_1+\lambda_2=\partial f/\partial C+\partial g/\partial R$ cannot be determined. Also, from $dR/dC]_{g(C)=0} > dR/dC]_{f(C)=0}$,

$$\left.\frac{dR}{dC}\right]_{g(C)=0} = -\frac{\partial g/\partial C}{\partial g/\partial R} > \left.\frac{dR}{dC}\right]_{f(C)=0} = -\frac{\partial f/\partial C}{\partial f/\partial R} \Rightarrow \lambda_1\lambda_2 = \frac{\partial f}{\partial C}\frac{\partial g}{\partial R} - \frac{\partial f}{\partial R}\frac{\partial g}{\partial C} > 0,$$

as expected from any complex conjugate eigenvalues.

To investigate how the sign of the real parts of the complex eigenvalues varies with respect to $k_1(A)$, the characteristic equation for $D\Phi(\bar{X})$ ($|D\Phi(\bar{X})-\lambda I|$) was solved numerically. The numerical solution shows that there are two negative eigenvalues and a pair of conjugate complex eigenvalues. Figure 11 shows the location of conjugate eigenvalues in the complex plane. The stable steady state loses stability via a Hopf bifurcation as a pair of conjugate eigenvalues crosses the imaginary axis at $k_1=0.65$. At about 0.7 the pair merges to become real and remains so for $k_1=0.7-0.9$. Beyond $k_1\sim 0.9$, these eigenvalues become complex and the steady state regains stability near $k_1=1.85$. This corresponds to the transient with plateau-type Ca_i^{2+} response.[67]

This result suggests that for Ca_i^{2+} waves to be propagated to the neighboring cells, $k_1, k_{\mathrm{in}}(B_{\max}A/K_d+A)>0.6$ is required in each cells. However, under nonregenerative ATP release assumption, extracellular ATP is attenuated due to diffusion and enzymes as it propagates, and eventually $k_{\mathrm{in}}(B_{\max}A/K_d+A)$ becomes less than 0.6 ($A<2.5\ \mu M$; recall that the effective ATP dosage was 3 μM), at which the real part of complex conjugate eigenvalues becomes negative.

[1]Agulhon, C., Petravicz, J., McMullen, A. B., Sweger, E. J., Minton, S. K., Taves, S. R., Casper, K. B., Fiacco, T. A., and McCarthy, K. D., "What is the role of astrocyte calcium in neurophysiology?," Neuron **59**, 932–946 (2008).

[2]Anselmi, F., Hernandez, V. H., Crispino, G., Seydel, A., Ortolano, S., Roper, S. D., Kessaris, N., Richardson, W., Rickheit, G., Filippov, M. A., Monyer, H. , and Mammano, F., ATP release through connexin hemichannels and gap junction transfer of second messengers propagate Ca^{2+} signals across the inner ear," Proc. Natl. Acad. Sci. U.S.A. **105**, 18770–18775 (2008).

[3]Apolloni, S., Montilli, C., Finocchi, P., and Amadio, S., "Membrane compartments and purinergic signalling: P2x receptors in neurodegenerative and neuroinflammatory events," FEBS J. **276**, 354–364 (2009).

[4]Arcuino, G., Lin, J. H.-C., Takano, T., Liu, C., Jiang, L., Gao, Q., Kang, J., and Nedergaard, M., "Intercellular calcium signaling mediated by point-source burst release of ATP," Proc. Natl. Acad. Sci. U.S.A. **99**, 9840–9845 (2002).

[5]Aronson, D. G., Mantzaris, N. V., and Othmer, H. G., "Wave propagation and blocking in inhomogeneous media," Discrete Contin. Dyn. Syst. **13**, 843–876 (2005).

[6]Ashida, N., Ueyama, T., Rikitake, K., Shirai, Y., Eto, M., Kondoh, T., Kohmura, E., and Saito, N., "Ca^{2+} oscillation induced by P2Y2 receptor activation and its regulation by a neuron-specific subtype of PKC (gamma PKC)," Neurosci. Lett. **446**, 123–128 (2008).

[7]Atri, A., Amundson, J., Clapham, D., and Sneyd, J., "A single-pool model for intracellular calcium oscillations and waves in the xenopus laevis oocyte," Biophys. J. **65**, 1727–1739(1993).

[8]Babwah, A. V., Dale, L. B., and Ferguson, S. S. G., "Protein kinase C isoform-specific differences in the spatial-temporal regulation and decoding of metabotropic glutamate receptor1a-stimulated second messenger responses," J. Biol. Chem. **278**, 5419–5426 (2003).

[9]Barrow, S. L., Sherwood, M. W., Dolman, N. J., Gerasimenko, O. V., Voronina, S. G., and Tepikin, A. V., "Movement of calcium signals and calcium-binding proteins: Firewalls, traps and tunnels," Biochem. Soc. Trans. **34**, 381–384 (2006).

[10]Bartlett, P. J., Young, K. W., Nahorski, S. R., and Challiss, R. A. J., "Single cell analysis and temporal proling of agonist-mediated inositol 1,4,5-trisphosphate, Ca^{2+}, diacylglycerol, and protein kinase C signaling using fluorescent biosensors," J. Biol. Chem. **280**, 21837–21846 (2005).

[11]Bennett, M. R., Buljan, V., Farnell, L., and Gibson, W. G., "Purinergic junctional transmission and propagation of calcium waves in spinal cord astrocyte networks," Biophys. J. **91**, 3560–3571 (2006).

[12]Bennett, M. R., Farnell, L., and Gibson, W. G., "A quantitative model of cortical spreading depression due to purinergic and gap-junction transmission in astrocyte networks," Biophys. J. **95**, 5648–5660 (2008).

[13]Berridge, M. J., Bootman, M. D., and Lipp, P., "Calcium—A life and death signal," Nature (London) **395**, 645–648 (1998).

[14]Bezprozvanny, I., Watras, J., and Ehrlich, B. E., "Bell-shaped calcium-response curves of ins(1,4,5)p3- and calcium-gated channels from endoplasmic reticulum of cerebellum," Nature (London) **351**, 751–754 (1991).

[15]Blomstrand, F., Aberg, N. D., Eriksson, P. S., Hansson, E., and Rönnbäck, L., "Extent of intercellular calcium wave propagation is related to gap junction permeability and level of connexin-43 expression in astrocytes in primary cultures from four brain regions," Neuroscience **92**, 255–265 (1999).

[16]Bobalova, J. and Mutafova-Yambolieva, V. N., "Co-release of endogenous ATP and noradrenaline from guinea-pig mesenteric veins exceeds co-release from mesenteric arteries," Clin. Exp. Pharmacol. Physiol. **28**, 397–401 (2001).

[17]Bowser, D. N. and Khakh, B. S., "Two forms of single-vesicle astrocyte exocytosis imaged with total internal reflection fluorescence microscopy," Proc. Natl. Acad. Sci. U.S.A. **104**, 4212–4217 (2007).

[18]Bowser, D. N. and Khakh, B. S., "Vesicular ATP is the predominant cause of intercellular calcium waves in astrocytes," J. Gen. Physiol. **129**, 485–491 (2007).

[19]Braet, K., Aspeslagh, S., Vandamme, W., Willecke, K., Martin, P. E. M., Evans, W. H., and Leybaert, L., "Pharmacological sensitivity of ATP release triggered by photoliberation of inositol-1,4,5-trisphosphate and zero extracellular calcium in brain endothelial cells," J. Cell Physiol. **197**, 205–213 (2003).

[20]Braet, K., Vandamme, W., Martin, P. E. M., Evans, W. H., and Leybaert, L., "Photoliberating inositol-1,4,5-trisphosphate triggers ATP release that is blocked by the connexin mimetic peptide gap 26," Cell Calcium **33**, 37–48 (2003).

[21]Bushong, E. A., Martone, M. E., Jones, Y. Z., and Ellisman, M. H., "Protoplasmic astrocytes in CA1 stratum radiatum occupy separate anatomical domains," J. Neurosci. **22**, 183–192 (2002).

[22]Coco, S., Calegari, F., Pravettoni, E., Pozzi, D., Taverna, E., Rosa, P., Matteoli, M., and Verderio, C., "Storage and release of ATP from astrocytes in culture," J. Biol. Chem. **278**, 1354–1362 (2003).

[23]Codazzi, F., Teruel, M. N., and Meyer, T., "Control of astrocyte Ca^{2+} oscillations and waves by oscillating translocation and activation of protein kinase C," Curr. Biol. **11**, 1089–1097 (2001).

[24]Cornell-Bell, A. H., Finkbeiner, S. M., Cooper, M. S., and Smith, S. J., "Glutamate induces calcium waves in cultured astrocytes: Long-range glial signaling," Science **247**, 470–473 (1990).

[25]Cotrina, M. L., Lin, J. H., Alves-Rodrigues, A., Liu, S., Li, J., Azmi-Ghadimi, H., Kang, J., Naus, C. C., and Nedergaard, M., "Connexins regulate calcium signaling by controlling ATP release," Proc. Natl. Acad. Sci. U.S.A. **95**, 15735–15740 (1998).

[26]Cotrina, M. L., Lin, J. H.-C., López-García, J. C., Naus, C. C. G., and Nedergaard, M., "ATP-mediated glia signaling," J. Neurosci. **20**, 2835–2844 (2000).

[27]Cotrina, M. L., Lin, J. H.-C., and Nedergaard, M., "Cytoskeletal assembly and ATP release regulate astrocytic calcium signaling," J. Neurosci. **18**, 8794–8804 (1998).

[28]Cunningham, M. L., Filtz, T. M., and Harden, T. K., "Protein kinase C-promoted inhibition of galpha(11)-stimulated phospholipase C-beta activity," Mol. Pharmacol. **56**, 265–271 (1999).

[29]Dale, L. B., Babwah, A. V., Bhattacharya, M., Kelvin, D. J., and Ferguson, S. S., "Spatial-temporal patterning of metabotropic glutamate receptor-mediated inositol 1,4,5-triphosphate, calcium, and protein kinase C oscillations: Protein kinase C-dependent receptor phosphorylation is not required," J. Biol. Chem. **276**, 35900–35908 (2001).

[30]Dale, L. B., Babwah, A. V., and Ferguson, S. S. G., "Mechanisms of metabotropic glutamate receptor desensitization: Role in the patterning of

eector enzyme activation," Neurochem. Int. **41**, 319–326 (2002).
[31]Dale, L. B., Bhattacharya, M., Anborgh, P. H., Murdoch, B., Bhatia, M., Nakanishi, S., and Ferguson, S. S., "G protein-coupled receptor kinase-mediated desensitization of metabotropic glutamate receptor 1a protects against cell death," J. Biol. Chem. **275**, 38213–38220 (2000).
[32]Davalos, D., Grutzendler, J., Yang, G., Kim, J. V., Zuo, Y., Jung, S., Littman, D. R., Dustin, M. L., and Gan, W. B., "ATP mediates rapid microglial response to local brain injury *in vivo*," Nat. Neurosci. **8**, 752–758 (2005).
[33]Davis, T. and Duff, I., "An unsymmetric-pattern multifrontal method for sparse LU factorization," SIAM J. Matrix Anal. Appl. **18**, 140–158 (1997).
[34]Delicado, E., Jimenez, A., Carrasquero, L., Castro, E., and Miras-Portugal, M., "Cross-talk among epidermal growth factor, ap (5) a, and nucleotide receptors causing enhanced ATP Ca^{2+} signaling involves extracellular kinase activation in cerebellar astrocytes," J. Neurosci. Res. **81**, 789–796 (2005).
[35]Ding, S., Fellin, T., Zhu, Y., Lee, S. Y., Auberson, Y. P., Meaney, D. F., Coulter, D. A., Carmignoto, G., and Haydon, P. G., "Enhanced astrocytic Ca^{2+} signals contribute to neuronal excitotoxicity after status epilepticus," J. Neurosci. **27**, 10674–10684 (2007).
[36]Dokukina, I., Gracheva, M., Grachev, E., and Gunton, J., "Role of network connectivity in intercellular calcium signaling," Physica D **237**, 745–754 (2008).
[37]Dupont, G., Combettes, L., and Leybaert, L., "Calcium dynamics: Spatio-temporal organization from the subcellular to the organ level," Int. Rev. Cytol. **261**, 193–245 (2007).
[38]Dupont, G. and Goldbeter, A., "Oscillations and waves of cytosolic calcium: Insights from theoretical models," BioEssays **14**, 485–493 (1992).
[39]Dupont, G. and Goldbeter, A., "Properties of intracellular Ca^{2+} waves generated by a model based on Ca^{2+}-induced Ca^{2+} release," Biophys. J. **67**, 2191–2204 (1994).
[40]Espallergues, J., Solovieva, O., Técher, V., Bauer, K., Alonso, G., Vincent, A., and Hussy, N., "Synergistic activation of astrocytes by ATP and norepinephrine in the rat supraoptic nucleus," Neuroscience **148**, 712–723 (2007).
[41]Falcke, M., Li, Y., Lechleiter, J. D., and Camacho, P., "Modeling the dependence of the period of intracellular Ca^{2+} waves on serca expression," Biophys. J. **85**, 1474–1481 (2003).
[42]Fall, C. P., Wagner, J. M., Loew, L. M., and Nuccitelli, R., "Cortically restricted production 1 of IP_3 leads to propagation of the fertilization Ca^{2+} wave along the cell surface in a model of the xenopus egg," J. Theor. Biol. **231**, 487–496 (2004).
[43]Fiacco, T. A., Agulhon, C., Taves, S. R., Petravicz, J., Casper, K. B., Dong, X., Chen, J., and McCarthy, K. D., "Selective stimulation of astrocyte calcium *in situ* does not affect neuronal excitatory synaptic activity," Neuron **54**, 611–626 (2007).
[44]Fiacco, T. A. and McCarthy, K. D., "Intracellular astrocyte calcium waves *in situ* increase the frequency of spontaneous ampa receptor currents in CA1 pyramidal neurons," J. Neurosci. **24**, 722–732 (2004).
[45]Fiacco, T. A. and McCarthy, K. D., "Astrocyte calcium elevations: Properties, propagation, and effects on brain signaling," Glia **54**, 676–690 (2006).
[46]Filtz, T. M., Cunningham, M. L., Stanig, K. J., Paterson, A., and Harden, T. K., "Phosphorylation by protein kinase C decreases catalytic activity of avian phospholipase C-beta," Biochem. J. **338**, 257–264 (1999).
[47]Fowler, A. C., *Mathematical Models in the Applied Sciences* (Cambridge University Press, Cambridge, UK, 1997).
[48]Franke, H., Krügel, U., Grosche, J., Heine, C., Härtig, W., Allgaier, C., and Illes, P., "P2Y receptor expression on astrocytes in the nucleus accumbens of rats," Neuroscience **127**, 431–441 (2004).
[49]Giaume, C. and Venance, L., "Intercellular calcium signaling and gap junctional communication in astrocytes," Glia **24**, 50–64 (1998).
[50]Gordon, J. L., "Extracellular ATP: effects, sources and fate," Biochem. J. **233**, 309–319 (1986).
[51]Gribble, F. M., Loussouarn, G., Tucker, S. J., Zhao, C., Nichols, C. G., and Ashcroft, F. M., "A novel method for measurement of submembrane ATP concentration," J. Biol. Chem. **275**, 30046–30049 (2000).
[52]Griffith, D. A. and Jarvis, S. M., "Nucleoside and nucleobase transport systems of mammalian cells," Biochim. Biophys. Acta **1286**, 153–181 (1996).
[53]Guan, X., Cravatt, B. F., Ehring, G. R., Hall, J. E., Boger, D. L., Lerner, R. A., and Gilula, N. B., "The sleep-inducing lipid oleamide deconvolutes gap junction communication and calcium wave transmission in glial cells," J. Cell Biol. **139**, 1785–1792 (1997).
[54]Guthrie, P. B., Knappenberger, J., Segal, M., Bennett, M. V. L., Charles, A. C., and Kater, S. B., "ATP released from astrocytes mediates glial calcium waves," J. Neurosci. **19**, 520–528 (1999).
[55]Hall, J., *Guyton Physiology Review* (Saunders, 2005).
[56]Hamilton, N., Vayro, S., Kirchhoff, F., Verkhratsky, A., Robbins, J., Gorecki, D., and Butt, A., "Mechanisms of ATP-and glutamate-mediated calcium signaling in white matter astrocytes," Glia **56**, 734–749 (2008).
[57]Harris-White, M. E., Zanotti, S. A., Frautschy, S. A., and Charles, A. C., "Spiral intercellular calcium waves in hippocampal slice cultures," J. Neurophysiol. **79**, 1045–1052 (1998).
[58]Hassinger, T. D., Guthrie, P. B., Atkinson, P. B., Bennett, M. V., and Kater, S. B., "An extracellular signaling component in propagation of astrocytic calcium waves," Proc. Natl. Acad. Sci. U.S.A. **93**, 13268–13273 (1996).
[59]Hubley, M. J., Locke, B. R., and Moerland, T. S., "The effects of temperature, pH, and magnesium on the diffusion coefficient of ATP in solutions of physiological ionic strength," Biochim. Biophys. Acta **1291**, 115–121 (1996).
[60]Höfer, T., Venance, L., and Giaume, C., "Control and plasticity of intercellular calcium waves in astrocytes: A modeling approach," J. Neurosci. **22**, 4850–4859 (2002).
[61]Jafri, M. S. and Keizer, J., "On the roles of Ca^{2+} diffusion, Ca^{2+} buffers, and the endoplasmic reticulum in IP_3-induced Ca^{2+} waves," Biophys. J. **69**, 2139–2153 (1995).
[62]Jafri, M. S. and Keizer, J., "Agonist-induced calcium waves in oscillatory cells: A biological example of Burgers' equation," Bull. Math. Biol. **59**, 1125–1144 (1997).
[63]John, G. R., Scemes, E., Suadicani, S. O., Liu, J. S., Charles, P. C., Lee, S. C., Spray, D. C., and Brosnan, C. F., "Il-1beta differentially regulates calcium wave propagation between primary human fetal astrocytes via pathways involving P2 receptors and gap junction channels," Proc. Natl. Acad. Sci. U.S.A. **96**, 11613–11618 (1999).
[64]Joseph, S. M., Buchakjian, M. R., and Dubyak, G. R., "Colocalization of ATP release sites and ecto-ATPase activity at the extracellular surface of human astrocytes," J. Biol. Chem. **278**, 23331–23342 (2003).
[65]Kang, J., Kang, N., Lovatt, D., Torres, A., Zhao, Z., Lin, J., and Nedergaard, M., "Connexin 43 hemichannels are permeable to ATP," J. Neurosci. **28**, 4702–4711 (2008).
[66]Kang, M., "Temporal and spatial aspects of calcium dynamics in astrocytes," Ph.D. thesis, University of Minnesota, 2004.
[67]Kang, M. and Othmer, H. G., "The variety of cytosolic calcium responses and possible roles of PLC and PKC," Phys. Biol. **4**, 325–343 (2007).
[68]Katsuragi, T., Sato, C., Usune, S., Ueno, S., Segawa, M., and Migita, K., "Caffeine-inducible ATP release is mediated by Ca^{2+}-signal transducing system from the endoplasmic reticulum to mitochondria," Naunyn-Schmiedeberg's Arch. Pharmacol. **378**, 93–101 (2008).
[69]Kawano, S., Otsu, K., Kuruma, A., Shoji, S., Yanagida, E., Muto, Y., Yoshikawa, F., Hirayama, Y., Mikoshiba, K., and Furuichi, T., "ATP autocrine/paracrine signaling induces calcium oscillations and NFAT activation in human mesenchymal stem cells," Cell Calcium **39**, 313–324 (2006).
[70]Keener, J. and Sneyd, J., *Mathematical Physiology* (Springer, Berlin, 2001).
[71]Kimelberg, H. K., "Increased release of excitatory amino acids by the actions of ATP and peroxynitrite on volume-regulated anion channels (VRACs) in astrocytes," Neurochem. Int. **45**, 511–519 (2004).
[72]Konietzko, U. and Müller, C. M., "Astrocytic dye coupling in rat hippocampus: Topography, developmental onset, and modulation by protein kinase C," Hippocampus **4**, 297–306 (1994).
[73]Lazarowski, E. R., Watt, W. C., Stutts, M. J., Boucher, R. C., and Harden, T. K., "Pharmacological selectivity of the cloned human P2U-purinoceptor: potent activation by diadenosine tetraphosphate," Br. J. Pharmacol. **116**, 1619–1627 (1995).
[74]MacDonald, C. L., Yu, D., Buibas, M., and Silva, G. A., "Diffusion modeling of ATP signaling suggests a partially regenerative mechanism underlies astrocyte intercellular calcium waves," Front. Neuroeng. **1**, 1–13 (2008).
[75]Mazel, T., Richter, F., Vargová, L., and Syková, E., "Changes in extracellular space volume and geometry induced by cortical spreading depression in immature and adult rats," Physiol. Res. **51**, S85–S93 (2002).
[76]Merten, M. D., Saleh, A., Kammouni, W., Marchand, S., and Figarella, C., "Characterization of two distinct P2Y receptors in human tracheal gland cells," Eur. J. Biochem. **251**, 19–24 (1998).
[77]Mongin, A. A. and Kimelberg, H. K., "ATP potently modulates anion channel-mediated excitatory amino acid release from cultured astrocytes," Am. J. Physiol.: Cell Physiol. **283**, C569–C578 (2002).

[78]Nadkarni S., Jung P., and Levine H., "Astrocytes optimize the synaptic transmission of information," PLOS Comput. Biol. **4**, e1000088 (2008).
[79]Nagy, J. I. and Rash, J. E., "Connexins and gap junctions of astrocytes and oligodendrocytes in the CNS," Brain Res. Rev. **32**, 29–44 (2000).
[80]Nash, M. S., Schell, M. J., Atkinson, P. J., Johnston, N. R., Nahorski, S. R., and Challiss, R. A. J., "Determinants of metabotropic glutamate receptor-5-mediated Ca^{2+} and inositol 1,4,5-trisphosphate oscillation frequency. Receptor density versus agonist concentration," J. Biol. Chem. **277**, 35947–35960 (2002).
[81]Newman, E. A., Glial cells of the rat retina (http://www.manticmoo.com/articles/jeff/programming/latex/bibtextypes. php).
[82]Newman, E. A., "Propagation of intercellular calcium waves in retinal astrocytes and Müller cells," J. Neurosci. **21**, 2215–2223 (2001).
[83]Ni, Y., Malarkey, E. B., and Parpura, V., "Vesicular release of glutamate mediates bidirectional signaling between astrocytes and neurons," J. Neurochem. **103**, 1273–1284 (2007).
[84]Zur Nieden, R. Z. and Deitmer, J. W., "The role of metabotropic glutamate receptors for the generation of calcium oscillations in rat hippocampal astrocytes *in situ*," Cereb. Cortex **16**, 676–687 (2006).
[85]Oberheim, N. A., Wang, X., Goldman, S., and Nedergaard, M., "Astrocytic complexity distinguishes the human brain," Trends Neurosci. **29**, 547–553 (2006).
[86]Piet, R. and Jahr, C. E., "Glutamatergic and purinergic receptor-mediated calcium transients in Bergmann glial cells," J. Neurosci. **27**, 4027–4035 (2007).
[87]Piet, R., Vargová, L., Syková, E., Poulain, D. A., and Oliet, S. H. R., "Physiological contribution of the astrocytic environment of neurons to intersynaptic crosstalk," Proc. Natl. Acad. Sci. U.S.A. **101**, 2151–2155 (2004).
[88]De Pittà, M. D., Volman, V., Levine, H., Pioggia, G., Rossi, D. D., and Ben-Jacob, E., "Coexistence of amplitude and frequency modulations in intracellular calcium dynamics," Phys. Rev. E **77**, 030903(R) (2008).
[89]Porter, J. T. and McCarthy, K. D., "Astrocytic neurotransmitter receptors *in situ* and *in vivo*," Prog. Neurobiol. **51**, 439–455 (1997).
[90]Ralevic, V. and Burnstock, G., "Receptors for purines and pyrimidines," Pharmacol. Rev. **50**, 413–492 (1998).
[91]Rostovtseva, T. K. and Bezrukov, S. M., "ATP transport through a single mitochondrial channel, VDAC, studied by current fluctuation analysis," Biophys. J. **74**, 2365–2373 (1998).
[92]Sabirov, R. Z., Dutta, A. K., and Okada, Y., "Volume-dependent ATP-conductive large-conductance anion channel as a pathway for swelling-induced ATP release," J. Gen. Physiol. **118**, 251–266 (2001).
[93]Sanderson, M. J., Charles, A. C., Boitano, S., and Dirksen, E. R., "Mechanisms and function of intercellular calcium signaling," Mol. Cell Endocrinol. **98**, 173–187 (1994).
[94]Scemes, E., "Components of astrocytic intercellular calcium signaling," Mol. Neurobiol. **22**, 167–179 (2000).
[95]Scemes, E. and Giaume, C., "Astrocyte calcium waves: What they are and what they do," Glia **54**, 716–725 (2006).
[96]Sedaa, K. O., Bjur, R. A., Shinozuka, K., and Westfall, D. P., "Nerve and drug-induced release of adenine nucleosides and nucleotides from rabbit aorta," J. Pharmacol. Exp. Ther. **252**, 1060–1067 (1990).
[97]Shelton, M. K. and McCarthy, K. D., "Hippocampal astrocytes exhibit Ca^{2+}-elevating muscarinic cholinergic and histaminergic receptors *in situ*," J. Neurochem. **74**, 555–563 (2000).
[98]Shinozuka, K., Hashimoto, M., Masumura, S., Bjur, R. A., Westfall, D. P., and Hattori, K., "*In vitro* studies of release of adenine nucleotides and adenosine from rat vascular endothelium in response to alpha 1-adrenoceptor stimulation," Br. J. Pharmacol. **113**, 1203–1208 (1994).
[99]Silchenko, A. N. and Tass, P. A., "Computational modeling of paroxysmal depolarization shifts in neurons induced by the glutamate release from astrocytes," Biol. Cybern. **98**, 61–74 (2008).
[100]Sneyd, J., Girard, S., and Clapham, D., "Calcium wave propagation by calcium-induced calcium release: An unusual excitable system," Bull. Math. Biol. **55**, 315–344 (1993).
[101]Stamatakis, M. and Mantzaris, N. V., "Modeling of ATP-mediated signal transduction and wave propagation in astrocytic cellular networks," J. Theor. Biol. **241**, 649–668 (2006).
[102]Stamatakis, M. and Mantzaris, N. V., "Astrocyte signaling in the presence of spatial inhomogeneities," Chaos **17**, 033123-1–033123-12 (2007).
[103]Stout, C. E., Costantin, J. L., Naus, C. C. G., and Charles, A. C., "Intercellular calcium signaling in astrocytes via ATP release through connexin hemichannels," J. Biol. Chem. **277**, 10482–10488 (2002).
[104]Suadicani, S. O., Brosnan, C. F., and Scemes, E., "P2x7 receptors mediate ATP release and amplification of astrocytic intercellular Ca^{2+} signaling," J. Neurosci. **26**, 1378–1385 (2006).
[105]Suadicani, S. O., Flores, C. E., Urban-Maldonado, M., Beelitz, M., and Scemes, E., "Gap junction channels coordinate the propagation of intercellular Ca^{2+} signals generated by P2y receptor activation," Glia **48**, 217–229 (2004).
[106]Sykova, E., "The extracellular space in the CNS: Its regulation, volume and geometry in normal and pathological neuronal function," Neuroscientist **3**, 28–41 (1997).
[107]Tang, Y. and Othmer, H. G., "Frequency encoding in excitable systems with applications to calcium oscillations," Proc. Natl. Acad. Sci. U.S.A. **92**, 7869–7873 (1995).
[108]Taoufik, E. and Probert, L., "Ischemic neuronal damage," Curr. Pharm. Des. **14**, 3565–3573 (2008).
[109]Taylor, A. L., Kudlow, B. A., Marrs, K. L., Gruenert, D. C., Guggino, W. B., and Schwiebert, E. M., "Bioluminescence detection of ATP release mechanisms in epithelia," Am. J. Physiol. **275**, C1391–C1406 (1998).
[110]Thul, R., Bellamy, T. C., Roderick, H. L., Bootman, M. D., and Coombes, S., "Calcium oscillations," Adv. Exp. Med. Biol. **641**, 1–27 (2008).
[111]Tordjmann, T., Berthon, B., Claret, M., and Combettes, L., "Coordinated intercellular calcium waves induced by noradrenaline in rat hepatocytes: Dual control by gap junction permeability and agonist," EMBO J. **16**, 5398–5407 (1997).
[112]Uchino, M., Sakai, N., Kashiwagi, K., Shirai, Y., Shinohara, Y., Hirose, K., Iino, M., Yamamura, T., and Saito, N., "Isoform-specic phosphorylation of metabotropic glutamate receptor 5 by protein kinase C (PKC) blocks Ca^{2+} oscillation and oscillatory translocation of Ca^{2+}-dependent PKC," J. Biol. Chem. **279**, 2254–2261 (2004).
[113]Venance, L., Stella, N., Glowinski, J., and Giaume, C., "Mechanism involved in initiation and propagation of receptor-induced intercellular calcium signaling in cultured rat astrocytes," J. Neurosci. **17**, 1981–1992 (1997).
[114]Verkhratsky, A. and Kettenmann, H., "Calcium signalling in glial cells," Trends Neurosci. **19**, 346–352 (1996).
[115]Verkhratsky, A., Orkand, R. K., and Kettenmann, H., "Glial calcium: homeostasis and signaling function," Physiol. Rev. **78**, 99–141 (1998).
[116]Volman, V., Ben-Jacob, E., and Levine, H., "The astrocyte as a gatekeeper of synaptic information transfer," Neural Comput. **19**, 303–326 (2007).
[117]Volterra, A. and Meldolesi, J., "Astrocytes, from brain glue to communication elements: The revolution continues," Nat. Rev. Neurosci. **6**, 626–640 (2005).
[118]De Vuyst, E. D., Decrock, E., Cabooter, L., Dubyak, G. R., Naus, C. C., Evans, W. H., and Leybaert, L., "Intracellular calcium changes trigger connexin hemichannel opening," EMBO J. **25**, 34–44 (2006).
[119]Wagner, J., Li, Y. X., Pearson, J., and Keizer, J., "Simulation of the fertilization Ca^{2+} wave in xenopus laevis eggs," Biophys. J. **75**, 2088–2097 (1998).
[120]Wang, Z., Haydon, P. G., and Yeung, E. S., "Direct observation of calcium-independent intercellular ATP signaling in astrocytes," Anal. Chem. **72**, 2001–2007 (2000).
[121]Wilson, P. D., Hovater, J. S., Casey, C. C., Fortenberry, J. A., and Schwiebert, E. M., "ATP release mechanisms in primary cultures of epithelia derived from the cysts of polycystic kidneys," J. Am. Soc. Nephrol. **10**, 218–229 (1999).
[122]Zhang, Z., Chen, G., Zhou, W., Song, A., Xu, T., Luo, Q., Wang, W., Gu, X., and Duan, S., "Regulated ATP release from astrocytes through lysosome exocytosis," Nat. Cell Biol. **9**, 945–953 (2007).
[123]Zhao, Y., Migita, K., Sato, C., Usune, S., Iwamoto, T., and Katsuragi, T., "Endoplasmic reticulum is a key organella in bradykinin-triggered ATP release from cultured smooth muscle cells," J. Pharmacol. Sci. **105**, 57–65 (2007).